Interpreting Brain Activation by Pattern Classification and Connectivity Analysis

A Thesis Submitted in partial fulfillment of the requirement for the Degree of Master of Technology in Intelligent Automation and Robotics

Department of Electronics and Telecommunication Engineering,
Jadavpur University
May 31, 2019

By
Dipayan Dewan
Registration No.:137308 of 2016-17
Roll No.:M6IAR19017

Under the guidance of
Prof. Amit Konar

Department of Electronics and Telecommunication Engineering,
Jadavpur University, Kolkata-700032

CERTIFICATE

This is to certify that that the dissertation entitled "**Interpreting Brain Activation by Pattern Classification and Connectivity Analysis**" has been carried out Dipayan Dewan (University Registration No: 137308 of 2016-2017) under my guidance and supervision and be accepted in partial fulfillment of the requirement for the Degree of Master of Electronics & Telecommunication Engineering. The research results presented in the thesis have not been included in any other paper submitted for the award of any degree to any other University or Institute.

_____

Prof. AmitKonar(Supervisor)Dept.
of Electronics & Telecommunication Engineering
Jadavpur University

_____

Prof. Sheli Sinha Chaudhuri
Head of the Department
Electronics & Telecommunication Engineering
Jadavpur University

_____

Prof. Chiranjib Bhattacharjee
Dean, Faculty Council of Engineering and
Technology Jadavpur University

FACULTY OF ENGINEERING AND TECHNOLOGY

JADAVPUR UNIVERSITY

CERTIFICATE OF APPROVAL*

The forgoing thesis is hereby approved as a creditable study of an engineering subject and presented in a manner satisfactory to warrant acceptance as prerequisite to the degree for which it has been submitted. It is understood that by this approval the undersigned do not necessarily endorse or approve any statement made, opinion expressed or conclusion drawn there in but approve the thesis only for which it is submitted.

Committee on final examination

For the evaluation of the thesis

_____

Signature of the Examiner

*Only in the case the thesis is approved

FACULTY OF ENGINEERING AND TECHNOLOGY

JADAVPUR UNIVERSITY

DECLARATION OF ORIGINALITY AND COMPLIANCE OFACADEMIC THESIS

I hereby declare that the thesis entitled "**Interpreting Brain Activation by Pattern Classification and Connectivity Analysis**" contains literature survey and original research work by the undersigned candidate, as part of his Degree of Master of Electronics & Telecommunication Engineering.

All information have been obtained and presented with academic rules and ethical conduct.

I also declare that, as required by these rules and conduct, I have fully cited and referenced all materials and results that are not original to this work.

Name: DIPAYAN DEWAN

Class RollNo: 001610704020

Thesis Title: Interpreting Brain Activation by Pattern Classification and Connectivity Analysis

_____

Signature of the candidate

ACKNOWLEDGEMENT

First and foremost, I would like to express my earnest gratitude and heartfelt indebtedness to my advisor, Prof. Amit Konar, Department of Electronics and Telecommunication Engineering, for the privilege and the pleasure, of allowing me to work under him towards my Degree of Master of Technology in Intelligent Automation and Robotics under Electronics and Telecommunication Engineering department. This work would not have been materialized, but for his whole-hearted help and support. Working under him has been a great experience. I sincerely thank my supervisor, particularly for all the faith he had in me.

I am thankful to Prof. Sheli Sinha Chaudhuri who has acted as Head of the Department of Electronics and Telecommunication Engineering during the tenure of my studentship. I would also like to show my special gratitude to Ms. Lidia Ghosh, PhD Research Scholar of the Department of Electronics and Telecommunication Engineering(ETCE), for her constant guidance and valuable advices. I would also like to thank Mr. Abir Chowdhury, M.Tech student and Mr. Biswadeep Chackroborty, Mr. Saptak Ghoshal, B.E student of the Department of ETCE for theire help in my work throughout the time.

My special thanks goes to Mr. Animesh Saha, M. Tech. student of Nantechnology department from Jadavpur University. Lastly, I would like to thank my parents for their love, support and guidance through the course work.

Dipayan Dewan

PREFACE

Color perception in human visual system is a well known problem. When dealing with this, the reason is still unknown. All the visible color are combination of three primary color Red, Green and Blue. Human who are facing problem to correctly determine the color is our main area of interest. Here we propose a technique to detect the brain signaling pathaway, during subjective engagement of color perception. Here a couple of method is demonstrated to determine the signaling pathway of brain signal using causality check between different brain lobe from collected EEG data. First two topic of this thesis is deals with the above mention problem with different technique.

The last application is concern with a completely different topic. In this topic we approached a way to classify human behavioral nature. Human behavior can be classified into two broad class on the basis of their thinking during a decision making task. We use a powerful Deep Neural Network based classifier to classify the human category.

Contents

List of Figures

List of Tables

Chapter 1

Introduction to Brain Computer Interface

Abstract

A brain-computer interface is the mode of direct communication between a wired brain and an external device. Since its inception in the 1970s, it has been widely used by researchers all over the world to understand human behavior and psychology. The BCI community over the years has seen substantial amount of work done on BCI technologies and many successful BCI applications. However, continuous efforts to further optimize and improve the capabilities, usability and robustness of these systems for use in humans is still needed. This chapter sheds light on the state-of-the-art of BCI as an emerging human-computer interaction technology.

1.1 Introduction

Individuals with healthy motor functions may take for granted the complicated biological, chemical, and electrical processes that occur within their body in order for them to easily communicate and interact with the outside world. Although the processes are complex, healthy individuals are able to complete them without much thought or effort. However, when certain neuron pathways are severed or degeneration brought on by an injury or a disease occurs, what once were simple tasks may become impossible or very cumbersome to complete.

The research on BCIs began in the 1970's at the University of California, Los Angeles under the grant from the National Science Foundation. The current goal of BCI research is to develop replacement communication and control means for severely disabled people. For those who have lost all voluntary muscle control, referred to as locked-in syndrome, BCI technology offers the only means of communication or environment control. Furthermore, BCI has applications in facilitating those with cognitively intact but severe motor impairments to write sentences, play video games, perform collaborative work, and create arts, through brain signal processing and interpretation.

BCI systems consist of several sequential steps, which can be divided into four categories: brain activity pattern generation, signal acquisition, feature extraction, and classification. First, brain activity can be represented by electrical activity, magnetic fields created by electrical activity, and blood oxygenation, and it differs in spatial and temporal characteristics depending on stimulus type, stimulus intensity, mental effort, and mental status. Second, brain activity can be measured through various brain imaging techniques in the signal acquisition phase. The appropriate technique should be chosen according to the type of brain activity to be measured and the purpose of the measurement, largely divided into invasive and noninvasive methods. Third, in the feature extraction step, only the

important and interesting brain activities are extracted from the measured brain signals. Finally, the extracted brain features are analyzed through various algorithms to classify the user's current intention and status.

1.2 Steps Involved in BCI

1.2.1 Data Acquisition

The main purpose of this step is to acquire signals from brain activities using various types of sensors including electroencephalography (EEG), magnetoencephalography (MEG), electrocorticography (ECoG), electrical signal acquisition in single neurons (intracortical neural recording - INR), functional magnetic resonance imaging (fMRI), and functional near infrared spectroscopy (fNIRS). These brain data acquisition methods are evaluated by a few different criteria. Typical criteria include manner of deploying sensors, type of acquired signal, temporal resolution which is the ability to detect changes within a certain of time interval [1], spatial resolution which is the ability to detect source of changes in brain, and portability which is the ability to use acquisition device across different environments. Based on the technique of recording of brain data, neuroimaging methods are generally categorized by invasiveness of the recording technique and into two categories, namely, (1) noninvasive, and (2) invasive recording methods.

1.2.1.1 Noninvasive Recording Methods

A noninvasive recording technique uses sensors placed on the skin, such as the scalp, or machinery that surrounds the cranium in whole. Two types of noninvasive recording methods discussed in this section include (1) direct measures that detect electrical (e.g., EEG) or magnetic activity (e.g., MEG) of the brain, and (2) indirect measures of brain function reflecting brain metabolism or hemody-

namics of the brain (e.g., fMRI, fNIRS, and PET) that do not directly characterize the neuronal activity. Unlike invasive recording methods, these noninvasive techniques do not require surgery, internal chemical or machine implantation, or needle insertion in order to receive and record neural activity [2].

1. **Electroencephalography** : One of the most popular noninvasive neurophysiological recording techniques is electroencephalography, or EEG. This method measures electrical activity in the brain through the use of surface electrodes placed on the scalp [3]. The first human EEG was recorded by Hans Berger, a German psychiatrist, in 1924. The neurophysiological origin of EEG signals is the pyramidal neurons of the cortex [4]. An electrical impulse is sent down the axon and into the synapse every time neurons are fired during excitation. Since electrical signals are not able to cross neuronal boundaries, a chemical reaction is created between neurons. This chemical reaction is triggered by the electrical impulse and causes an action potential. An action potential is the process of neuron depolarization, followed by repolarization. Chemical information can begin flowing through the synaptic left when a neuron is at its resting polarization level. The flow causes the depolarization, and repolarization is necessary before more chemical information can flow through the synapse again . EEG measures the electrical current, which Teplan explained as that flow during synaptic excitations of the dendrites of many pyramidal neurons in the cerebral cortex. Because of the distance and impedance of bone and skin between the electrodes and the cerebral cortex, the EEG cannot accurately detect single neuron excitations. Instead, the EEG picks up local current flows on groups of active neurons within the cerebral cortex . Neural oscillations that are observed in EEG signals are popularly called brainwaves, reflecting different aspects when they occur in different locations in the brain. These

brain-waves are identified by frequency (in hertz or cycles per second) and amplitude in the range of microvolts (V or 1/1,000,000 of a volt). Each brainwave has its own set of characteristics representing a specific level of brain activity and mental states . For example, Delta brain-waves reflect slow, loud, and functional mental states that prevail during the late sleep , while the power decrease at the alpha band correlates to the presence of mental imagery. In order to record EEG signals, a head set consisting of an EEG cap with at least three electrodes (i.e., a ground, a reference, and a recording electrode) is needed (Figure 1.1b).

In addition, an amplifier, an A/D converter, and a computing device (such as a computer) are necessary. Electrodes are typically made of silver, silver chloride, or gold and can be considered wet, which requires conductive gel to be placed between electrode and scalp, or dry, where the electrode is placed directly onto the skin. Measurements from all electrodes are referred to one common electrode, called reference electrode. The active and reference electrodes serve as the signal receptors for potential difference comparisons. The ground electrode serves as the baseline of brainwave signals that helps weed out irrelevant data from the active and reference signals. Correct EEG electrode placement is important to ensure proper location of electrodes in relation to cortical areas so that they can be reliably and precisely maintained from individual to individual. The international 10/20 system has been an internationally recognized standard system for electrode positioning with 21 electrodes for half a century. Under the 10/20 system, the skull is divided into six areas from nasion to inion with interval rates of 10 % ,20%, 20%, 20%, 20%, and 10% (Fp: frontopolar, F: frontal, C: central, P: parietal, and O: occipital,respectively), and also divided into the same ratios from left to right pre-auricular points (T3: temporal, C3:

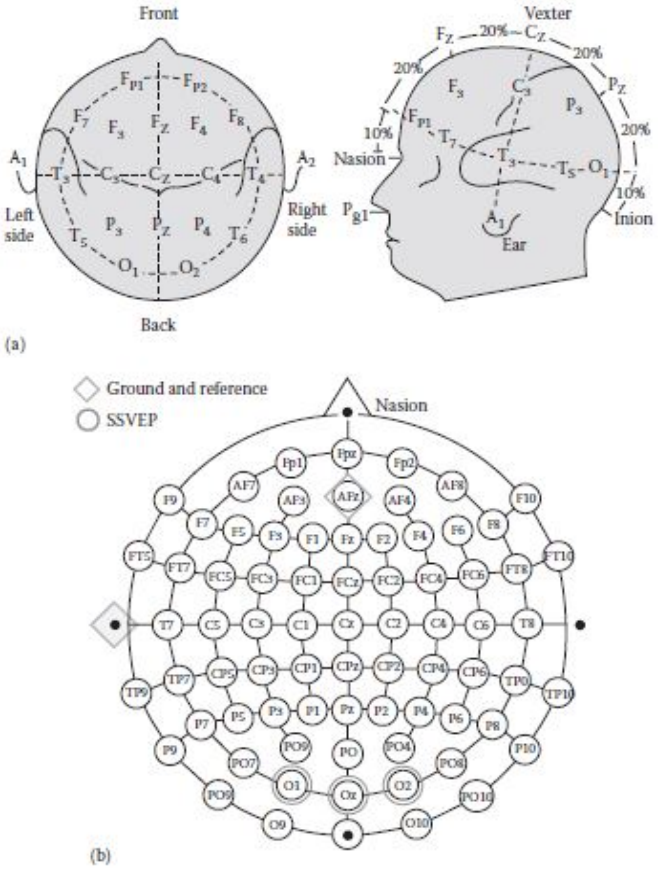

Figure 1.1: (a) The 10/20 international system of electrode placement. (b) An example montage based on the 10/10 system, which measures O1 and O2 with Oz bipolar method to elicit SSVEPs.

central, Cz, C4, and T5, respectively) (Klem et al. 1958). With the advent of multichannel EEG acquisition systems and the concurrent development of topographic and tomographic signal source localization methods, however, the international 10/20 system has been extended to higher-density electrode settings such as the 10/10 and 10/5 systems, allowing more than 500 electrode positions (for the effectiveness of 10/20-derived systems, see Jurcak et al. 2007). To accurately identify the location of scalp electrodes, anatomical landmarks should be determined for the essential positioning of the electrodes: (1) the nasion, which is the point between the forehead and the nose; (2) the inion, which is the lowest point of the skull from the back of the head and is normally indicated by a prominent bump; (3) the pre-auricular points anterior to the ear. The numbers 10 and 20 refer to the fact that the distances between adjacent electrodes are either 10% or 20% of the total frontback or rightleft distance of the skull. Each site has a letter to identify the lobe (i.e., F, T, C, P, and O stand for Frontal, Temporal, Central, Parietal, and Occipital, respectively), the Z(ero) to refer to an electrode placed on the midline, and a number to identify the hemisphere location (i.e., odd and even numbers referring to the left and right hemispheres, respectively). Also note that the smaller the number, the closer the position is to the midline. In Figure 1.4b, for example, electrode O1 identifies the left occipital, C4 identifies the right central, P3 identifies the left parietal, and A1 identifies the left ear reference. Currently, EEGs are among the most popular techniques for brain computer interfacing technology, making up 68% of BCI research articles published in 2007, 2011 as shown in Figure 1.2 [5]. It is noninvasive, inexpensive, and portable, making it a popular device in current research. It does not, however, provide high spatial quality information on the location of brain signal activation.

In addition, it is mathematically difficult to accurately compute the distribution of currents within the brain that generated these signals. This is referred to as the inverse problem.

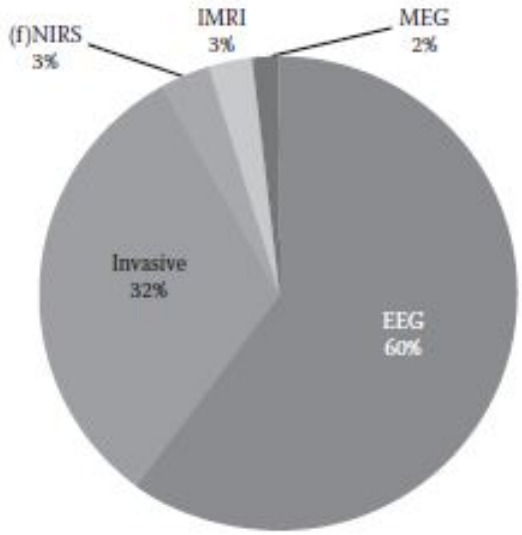

Figure 1.2: BCI research articles published in 2007–2011 from [5].

1.2.1.2 Invasive Recording Methods

Invasive recording methods are neuroimaging techniques in which the electrodes make direct contact with brain tissue. These methods can provide more accurate spatial and temporal information, but come at a greater risk to the individual. Two types of invasive recording methods are, namely, electrocorticography (ECoG) and intracortical neuron recording (INR).

1.2.2 Data Preprocessing

This step is very crucial to obtaining accurate BCIs. The acquired data must be pre-processed for noise and artefacts that are crept into the signal due to 50/60 Hz power supply interference, electrical noise from electronic components

and cable defects. Further, there are artefacts due to ocular and involuntary muscular activation. These artefact result in the recorded brain data to have low signal-to-noise ratio (SNR) and hence must be dealt with in a proper manner before going for further processes.

1.2.3 Feature Extraction

Feature extraction is a crucial step in the BCI scheme. Its task is to represent the whole signal by using some shorter and more meaningful measures called features [6] [7]. Until now, although there has been a lot of effort from neuroscientists seeking to discover brain and neural operations inside it, the overall knowledge of human-beings about the brain is still very limited. This shortcoming makes brain signal more difficult than other signals such as voice signal in feature extraction.

In this section, we describe a feature extraction procedure with an EEG-based SSVEP BCI example. Assume that there is a robot that can move four directions in a grid cell environment. A user can control the robot by gazing at one of four flashing LED stimuli (i.e., flickering at 7, 13, 17, and 23 Hz) that correspond to directional commands (up, down, left, and right, respectively). A starting position of the robot is randomly set and the user moves the robot via a BCI system to hit a target position. The robot moves one cell from its current location when the classification of BCI detects one of the four SSVEP features. The classification is made only if the amplitude of one of the frequencies exceeds a certain threshold within the most recent 5 s of EEG data. Otherwise, the robot will not move and will stay at its current position. EEG data record at a sampling rate of 512 Hz on the occipital area (O1 and O2). The recorded EEG data are first filtered by a 5-Hz high-pass filter, a 75-Hz low-pass filter, and a 60-Hz notch filter. The filtered EEG data are refined by the artifacts removal procedure, and subtract O1 channel to O2 channel by using the bipolar reference

method. Then, the EEG data are transformed into the frequency domain by fast Fourier transform (FFT). The time window for FFT is 5 s and a 1-s (512 data points) sliding time window is used, so one decision can be made every second. For each time window, the power values of the fundamental, second, and third harmonics for each frequency are summed up. For example, the power value of 23, 46, and 69 Hz will be summed up for the stimulus of 23 Hz. If the maximum power sum value among four values is two times bigger than the average of the others, then the robot will move one cell from its current location to the corresponding direction of the maximum power frequency. Otherwise, the robot stays in its current position. This procedure will continue until the robot arrives at the target position.

1.2.4 Feature Classification Methods

In the context of biomedical signal processing, especially with application to EEG signals, the classification of the data in feature spaces is often required. For example, to detect whether there is a left or right finger movement in the BCI area, the time, frequency and spatial features need to be classified. The objective of classification is to draw boundary between two or more classes and to label them based on their measured features. In a multi-dimenssional feature space, this boundary takes the form of a separating hyperplane. There have been several clustering and classification techniques developed within the last few years. Some well known and successful methods are Linear Discriminant Analysis (LDA), Principal Component Analysis (PCA), Support Vector Machine (SVM), Hidden Markov Model (HMM), k-nearest neighbours (kNN) and Artificial Neural Network (ANN). Among them, LDA and SVM are the two best classifiers [7].

1.3 Brain Signal Patterns for BCI Operation

Every BCI is created to respond to a certain type of brain signal. Figure 1.3 illustrates the most popular types of brain signals used for operating BCIs. What follows is an overarching review of the brain signal patterns in terms of their physiological bases, initial training requirement for use, and the rate at which information is transferred from brain to application. However, only neuroelectric signals, such as EEG, are discussed in the following sections, because it not only can cover most of brain patterns (P300, SSEP, and ERD/ERS) but also is the most studied BCI system because of its simplicity in application [3].

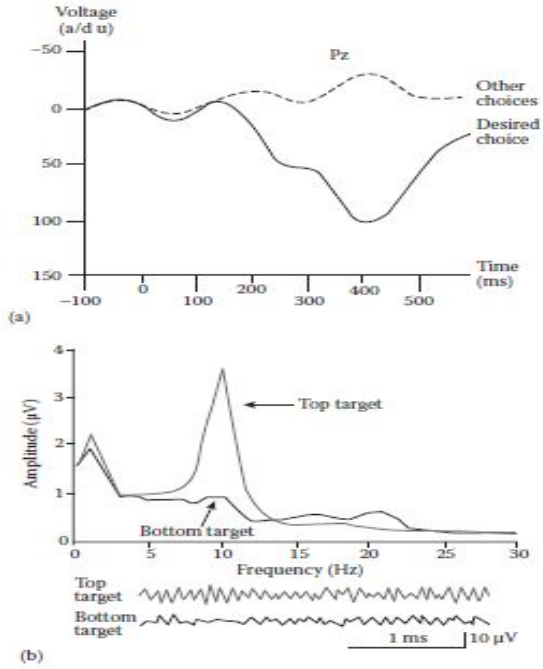

Figure 1.3: a) P300 ERP. b) Sensorimotor rhythm.

1.3.1 P300 ERPs

The P300 wave is a typical event related potential (ERP) component elicited in the process of decision making, which appeared just after 300 ms after the

event happened. It is considered to be an endogenous potential, as its occurrence links not to the physical attributes of a stimulus, but to a person's reaction to it. More specifically, the P300 is thought to reflect processes involved in stimulus evaluation or categorization. It is usually elicited using the oddball paradigm, in which low-probability target items are mixed with high-probability non-target (or "standard") items. When recorded by electroencephalography (EEG), it surfaces as a positive deflection in voltage with a latency (delay between stimulus and response) of roughly 250 to 500 ms. The signal is typically measured most strongly by the electrodes covering the parietal lobe. The presence, magnitude, topography and timing of this signal are often used as metrics of cognitive function in decision making processes. While the neural substrates of this ERP component still remain hazy, the reproducibility and ubiquity of this signal makes it a common choice for psychological tests in both the clinic and laboratory.To enable application of P300 for a P300 based BCI, the data have to be initially processed to reduce noise and enforce P-300-related information. A pattern recognition algorithm has to be developed later in order to check the presence of P300 wave in the recorded ERP epochs and label them.

1.3.2 Steady-State Evoked Potentials

An EEG evoked potential (EP) is a distinctive pattern of positive and negative voltage deflections that is time-locked to a specific sensory stimulus or event. Visual evoked potentials (VEPs) are those evoked by sudden visual stimuli, such as a light flash, the appearance of an image, or an abrupt change in color or pattern. Steady State VEPs (SSVEPs) [8] are stable oscillations in voltage that are elicited by rapid repetitive simulation such as a strobe light, an LED, or a pattern reversing checkerbox presented on a monitor. The successive stimulus presentations evoke similar responses, and the overlap of these responses

produces a steady state oscillation. The occipital region is the area where this feature is generated more prominently(shown in fig1.8). SSVEP is considered as a concept with two different definitions. Ragan proposed that SSVEP is a direct response in the primary visual cortex. On the other hand, Silberstein et al. assumed that the SSVEP includes indirect cortical responses via cortical-loops, from the peripheral retina, while a cognitive task is performed. SSVEP in this model has a complex amplitude and phase topography across the posterior scalp with considerable inter-subject variability. Although the main mechanism of SSVEP still is unknown, generally SSVEP is considered as a continuous visual cortical response evoked by repetitive stimuli with a constant frequency on the central retina. As a nearly sinusoidal oscillatory waveform, the SSVEP usually contains the same fundamental frequency as the stimulus and some harmonics of the fundamental frequency. For example, when the retina is excited by a visual stimulus at presentation rates ranging from 3.5 Hz to 75 Hz, the brain generates an electrical activity at the same and different frequency of the visual stimulus. The flickering stimulus of different frequency with a constant intensity can evoke the SSVEP in verity of amplitudes, ranging from (5-12Hz) as low frequencies, (12-25 Hz) as medium ones and (25-50 Hz) as high frequency bands. This type of stimulus is a powerful indicator in the diagnosis of visual pathway function, visual imperceptions.

SSVEP, along with evoked potentials , event-related potential(ERP), and sensorimotor rhythms, is widely adopted in current active and reactive BCIs. The SSVEP signal is a frequency-coded brain response that is generated as neurons of visual cortex synchronizing their firing to the frequency of continuous, repetitive visual stimulation. The main characteristics of SSVEP are frequency-locked and phase-locked. As the natural characteristics of SSVEPs, electrodes placed at the occipital region over the visual cortex can measure SSVEPs with high signal-to-

noise ratio(SNR). SSVEP amplitudes are sensitive to frequencies of visual flickers with predominant resonance peak at 30-80 Hz.

Due to the high signal-to noise (SNR) and relative immunity to artifacts, SSVEP has been widely used in diverse research fields including brain computer interface, visual attention, binocular rivalry and working memory. Using various techniques like EEG, MEG and fMRI, the related studies reveal that the SSVEP response is widely distributed over the occipital and other areas, including parietal, temporal, frontal, and prefrontal area. And these studies implicitly indicate that SSVEPs are the information integration of large- scale brain networks spanning across different cortical areas driven by flickering. Meanwhile, the pre-state EEG background has a large influence on cognitive processes, thus SSVEP responses may also be related to this baseline state.

1.3.3 ERD/ERS

Commonly, the EEG of the visual cortex is associated with the alpha rhythm, with its typical reactivity upon closing and opening the eyes. However, other types of rhythmic activities can be present in the same cortical areas, namely within the beta/gamma frequency range. With respect to the origin of beta/gamma rhythmic activity, several experimental facts have led to the interpretation that these rhythmic activities are primarily generated in the motor cortex as well as somato-sensory motor cortex itself (refer to the fig.10). These include the fact that sensory stimuli, cognitive tasks, motor tasks etc. induce changes in the EEG activity and accordingly these changes led to the oscillations in the beta/gamma frequency range, that are easily recorded from different cortical sites. These changes are basically event-related (ER), and reflect a decrease or an increase in the synchrony of the underlying neuronal populations. Alternatively, there may be an increase in the power corresponding to a certain frequency band known as

Event-Related Synchronization (ERS) or the decrease in the power corresponding to certain frequency band known as Event-Related Desynchronization (ERD) [8]. After a voluntary movement, the central cortex region exhibits a localized beta ERS. The exact frequency of this rebound beta ERS can vary considerably with the subject and type of movement. This beta ERS is observed not only after a real movement but also after an imagined movement. Furthermore, ERS in the gamma frequency band (around 35-40 Hz) can also be found over the central regions, preceding the execution of a movement, in contrast with the beta ERS, which has its maximum after the termination of the movement. When this form of ERS occurs, the excitability of the corticospinal pathways decreases, as revealed by means of transcranial magnetic stimulation [10]. This supports the hypothesis that the postmovement beta ERS corresponds to a deactivated state of the motor cortex. In contrast, the ERS in the gamma frequency band appears to reflect a state of active information processing. A desynchronized EEG means that in the underlying neural network or neuronal circuitry, small patches of neurons or neuronal assemblies work in a relative independent or desynchronized manner. In terms of information theory, a desynchronized system represents a state of maximal readiness and a maximum of information capacity. ERD can be followed by a beta rebound or beta ERS with a maximum within 1s after movement-offset (see, e.g. fig1.11). This time period corresponds to the occurrence of the post-movement beta ERS. This implies that the beta ERS with frequencies around 20 Hz can be interpreted, at least under certain circumstances, as a correlate of a deactivated cortical network.

1.4 Feature Classification Methods

One important element in BCI operations is a data classifier, or a classification algorithm, that aims at automatically determining a user's intention by classifying extracted brain features. Comprehensive reviews on the classification techniques used for BCIs have been given elsewhere(e.g., [6] [7] [9]). Thus, this section is restricted to present three types of the commonly employed classifiers to design EEG-based BCI systems and highlights their most important properties for BCI applications: linear classifiers, artificial neural network classifiers, and hidden Markov model classifiers.

1.4.1 Linear Classifiers

Linear classifiers are discriminant algorithms that use a linear function to classify the data into mutually exclusive and exhaustive classes, assuming that the data come from a Gaussian mixture model. Because of their structural simplicity, competitive accuracy, and very fast training and testing, linear classifiers are one of the most popular algorithms used to design BCI applications. Two main kinds of linear classifier are described: linear discriminant analysis (LDA) and support vector machine (SVM).

1.4.1.1 Linear Discriminant Analysis

The goal of the LDA technique is to project the original data matrix onto a lower dimensional space. To achieve this goal, three steps needed to be performed. The first step is to calculate the separability between different classes (i.e. the distance between the means of different classes), which is called the between-class variance or between-class matrix. The second step is to calculate the distance between the mean and the samples of each class, which is called the within-

class variance or within-class matrix. The third step is to construct the lower dimensional space which maximizes the between-class variance and minimizes the within-class variance.

1.4.1.2 Support Vector Machine

SVM is similar to LDA in that it is a binary classification algorithm that uses a discriminant hyperplane to distinguish two classes, but it is also different from LDA in that the selected best hyperplane for an SVM means the one with the largest margin (i.e., largest "gap" or "distance") between the classes. The data points that are closest to or on the separating hyperplane (a linear decision surface) are called support vectors. SVMs have several advantages because of theoretical reasons such as good generalization properties [10] and relative insensitive to overtraining [11] and the curse of dimensionality [12]. The disadvantages of SVMs include a poor performance if the number of features is much greater than the number of samples, an expensive n-fold cross-validation to calculate probability estimates, and a lower speed of execution [10]. In addition to performing linear classification, SVMs can efficiently classify nonlinearly separable data using what is called the kernel trick. This method uses a kernel function K(x,y) to implicitly map the data into another high-dimensional feature spaces. These RBF-based SVMs have been successfully applied to various BCI applications (e.g., [13]). In addition, SVMs have provided good empirical results for synchronous BCI problems (e.g., [13], motor imagery–based BCIs [14], P3 speller [15], and multiclass BCI problems using the OVR strategy [16].

1.5 Scope of the Thesis

Aim 1

Brain connectivity analysis using granger causality for primary color stimuli.

Objective 1

We provide a novel technique to determine the signal transduction pathway for color perception problem in 2-step. First the brain lobes having phase synchrony are identified by a frequency-domain analysis of the EEG signals acquired from 19 channels covering the entire sculp. Next, Granger causality is employed to determine the directional pathways on the basis of result obtained by phase synchrony analysis. Experiments undertaken on 10 subjects confirm that the color pathways in human beings are unique and distinct for the 3 primary colors: red, green and blue. The results obtained here from the research also supports the existing works reported on signal transduction pathways for colored light. The proposed method of detecting signal transduction pathways during color perception has immense applications in diagnosis of malfunctioning of one or more brain lobes residing on the pathway for people suffering from color blindness.

Aim 2

Brain connectivity analysis in color-perception problem using convergent cross mapping technique

Objective 2

Traditionally, Granger Causality analysis is employed to handle the problem. However, due to the applicability of Granger Causality analysis for purely stochas-

tic systems only, its suitability of applications in brain-connectivity analysis is limited due to the presence of both deterministic and stochastic characteristics in the human brain. Additionally, because of high parameter sensitivity of Granger Causality technique, identifying the right set of parameters itself poses an additional problem. Convergent cross mapping overcomes the above limitations and thus has immense scope for exploitation in brain-connectivity analysis. Here, we make an honest attempt to determine brain-connectivity during subjective engagement in color perception using convergent cross mapping technique. Experimental results envisage that the proposed technique yields precise brain-connectivity in color percerption in comparison to those obtained by the state-of-the-art techniques.

Aim 3

Decoding human decision making system using Convolutional Neural Network

Objective 3

Human behavior is a complex action which has provoked the thoughts of many people for a long time. However, little is currently known about the origin of cognition and the what defines a person's personality from another. In order to extract the features of a person's personality, we must at first be able to classify them based on their thought processes. In classical ethics, the people can be broadly classified into two main categories, namely, categorical and consequentialist. In this paper, we conduct several experiments where the users are faced with ethical dilemmas and the obtained brain EEG signals are used to classify them in the two categories using a novel modified Covolutional Neural Network. The results show that it is possible to indeed classify the people with extremely high accuracy with only their EEG signals. This provides scope for a new direction of research which

can be explored.

References

[1] B. Graimann, B. Allison, and G. Pfurtscheller, "Brain–computer interfaces: A gentle introduction," in *Brain-Computer Interfaces*, pp. 1–27, Springer, 2009. 3

[2] S. Bhattacharyya, A. Khasnobish, P. Ghosh, A. Mazumder, and D. Tibarewala, "A review on brain imaging techniques for bci applications," in *Medical Imaging: Concepts, Methodologies, Tools, and Applications*, pp. 300–330, IGI Global, 2017. 4

[3] E. Niedermeyer and F. L. da Silva, *Electroencephalography: basic principles, clinical applications, and related fields*. Lippincott Williams & Wilkins, 2005. 4, 11

[4] D. S. Cantor and J. R. Evans, *Clinical neurotherapy: application of techniques for treatment*. Academic Press, 2013. 4

[5] H.-J. Hwang, S. Kim, S. Choi, and C.-H. Im, "Eeg-based brain-computer interfaces: a thorough literature survey," *International Journal of Human-Computer Interaction*, vol. 29, no. 12, pp. 814–826, 2013. 6, 7, 8

[6] A. Bashashati, M. Fatourechi, R. K. Ward, and G. E. Birch, "A survey of signal processing algorithms in brain–computer interfaces based on electrical brain signals," *Journal of Neural engineering*, vol. 4, no. 2, p. R32, 2007. 9, 16

[7] F. Lotte, M. Congedo, A. Lécuyer, F. Lamarche, and B. Arnaldi, "A review

of classification algorithms for eeg-based brain–computer interfaces," *Journal of neural engineering*, vol. 4, no. 2, p. R1, 2007. 9, 10, 16

[8] G. Pfurtscheller, "Functional brain imaging based on erd/ers," *Vision research*, vol. 41, no. 10-11, pp. 1257–1260, 2001. 15

[9] L. F. Nicolas-Alonso and J. Gomez-Gil, "Brain computer interfaces, a review," *sensors*, vol. 12, no. 2, pp. 1211–1279, 2012. 16

[10] K. P. Bennett and C. Campbell, "Support vector machines: hype or hallelujah?," *Acm Sigkdd Explorations Newsletter*, vol. 2, no. 2, pp. 1–13, 2000. 17

[11] N. R. Pal and S. K. Pal, "A review on image segmentation techniques," *Pattern recognition*, vol. 26, no. 9, pp. 1277–1294, 1993. 17

[12] C. J. Burges, "A tutorial on support vector machines for pattern recognition," *Data mining and knowledge discovery*, vol. 2, no. 2, pp. 121–167, 1998. 17

[13] D. Garrett, D. A. Peterson, C. W. Anderson, and M. H. Thaut, "Comparison of linear, nonlinear, and feature selection methods for eeg signal classification," *IEEE Transactions on neural systems and rehabilitation engineering*, vol. 11, no. 2, pp. 141–144, 2003. 17

[14] H. Lee and S. Choi, "Pca+ hmm+ svm for eeg pattern classification," in *Seventh International Symposium on Signal Processing and Its Applications, 2003. Proceedings.*, vol. 1, pp. 541–544, IEEE, 2003. 17

[15] D. J. Krusienski, E. W. Sellers, F. Cabestaing, S. Bayoudh, D. J. McFarland, T. M. Vaughan, and J. R. Wolpaw, "A comparison of classification techniques

for the p300 speller," *Journal of neural engineering*, vol. 3, no. 4, p. 299, 2006. 17

[16] A. Schlögl, F. Lee, H. Bischof, and G. Pfurtscheller, "Characterization of four-class motor imagery eeg data for the bci-competition 2005," *Journal of neural engineering*, vol. 2, no. 4, p. L14, 2005. 17

Chapter 2

Brain Connectivity Analysis Using Granger Causality for Primary Color Stimuli

Abstract

This chapter provide a novel technique to determine the signal transduction pathway for color perception problem in 2-step. First the brain lobes having phase synchrony are identified by a frequency-domain analysis of the EEG signals acquired from 19 channels covering the entire sculp. Next, Granger causality is employed to determine the directional pathways on the basis of result obtained by phase-synchrony analysis. Experiments undertaken on 10 subjects confirm that the color pathways in human beings are unique and distinct for the 3 primary colors: red, green and blue. The results obtained here from the research also supports the existing works reported on signal transduction pathways for colored light. The proposed method of detecting signal transduction pathways during color perception has immense applications in diagnosis of malfunctioning

of one or more brain lobes residing on the pathway for people suffering from color blindness.

2.1 Introduction

Determining the signal transduction pathways in the brain is an interesting arena of research in modern brain sciences. [1]-[2] Although there exist traces of works on signal transduction pathways in the brain for different cognitive processes, there is a scarcity of research results on color pathways in the brain.[3]-[4] This paper proposes an interesting approach to determine the color processing pathways in the brain of the subjects by acquiring the EEG signals during the color processing phase of the subjects. The motivation is to determine whether for 3 basic colored lights brain follow the same or distinct signaling pathways by neural transduction process.

In order to perform the present analysis, two basic steps are undertaken on the acquired EEG signals after pre-processing and filtering. The steps include: i) phase synchrony analysis [5]- [6] and ii) Granger causality analysis [7]-[8] of the acquired EEG signals. The motivation of phase-synchrony analysis is to identify the signals significantly close in phase-space for a selected interval of time. In case two EEG signals acquired from electrodes E1 and E2 have close/similar phase values at all the sampling points of the selected interval, they are regarded to have a phase-synchrony. Naturally, at a given time point during color processing by the subject, quite a few channels are expected to show phase-synchrony. Although channels topographically close to each other have high likelihood to have phase synchrony, it is occasionally noted that channels spatially located far apart also have phase-synchrony. The characteristic of having phase-synchrony

in two or more channels spatially located apart carries important message about direct neural transduction pathways between distinct lobes. Although the phase-synchrony analysis provides the neural basis of brain-lobe connectivity during the color perceptual-process, it hardly can offer any information about direction of signal-flow between pairs of lobes. Fortunately, there exist several approaches to determine the directional connectivity between pairs of signal sources and sinks. A few among them that need special mention includes Granger causality [7]-[8], transfer-entropy [9] and cross-correlation [10] techniques. Granger causality analysis aims at determining the influence of one stationary signal on a second one. Transfer-entropy measures the information-transfer from one signal to the other. Granger causality is preferred to other existing approaches of signal directivity analysis for its high time-efficiency. This inspired the authors to employ Granger causality analysis to label the directivity in the edges of the unlabelled edged-graph obtained by phase-synchrony analysis. Ultimately, a directed graph is obtained during the perceptual process of 3 basic colors: red, green and blue. It is interesting to note that the graphs obtained by the above process have dissimilarity, signifying the involvement of different lobes at different time points during perception of the basic colors.

The significance of the present work is 2-fold. First, this paper demonstrates a novel approach to determine the signal transduction pathways in color perceptual processes. This might be utilized as a diagnostic tool to determine the brain lobes unable to participate in the generic signal transduction pathways used for analysis of color-perception. It also opens up a new vista of knowledge that the signal transduction pathways for 3 basic colors are distinct, thereby interpreting a parallel pathways for multi-colored information processing.

2.2 Principle and methodology

To determine the functional connectivity and signaling pathway for the color perception problem in between the different lobe of the human brain, phase synchrony and granger causality analysis is performed. The overall system is represented here in a block diagram in Figure 2.1.

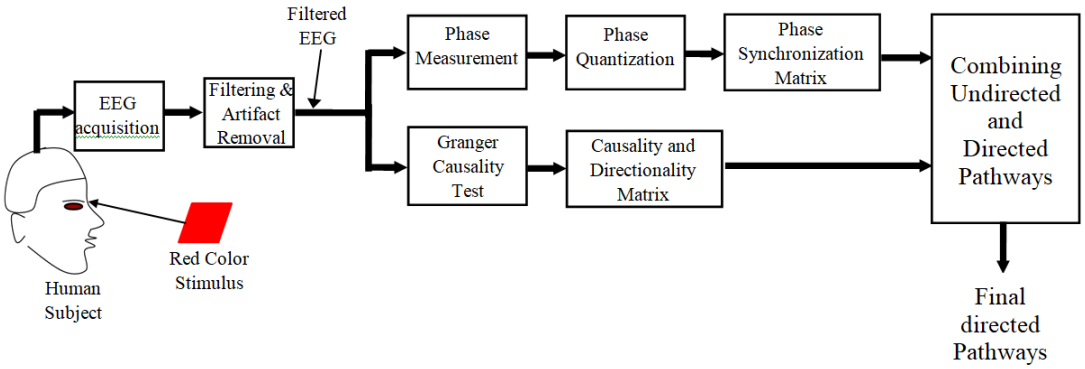

Figure 2.1: Block diagram of overall system

2.2.1 Phase computation of an EEG signals

Given a time-domain signal x(t), we obtain Fourier transform of x(t) to gain frequency-domain information. Finally

$$F\{f(t)\} = \mathbb{R}\mathrm{e}\{t\} + j\,\mathbb{I}\mathrm{m}\{t\} \tag{2.1}$$

where $\mathbb{R}\mathrm{e}\{t\}$ and $\mathbb{I}\mathrm{m}\{t\}$ are real. The phase information of $F\{f(t)\}$ is given by $\phi(t) = tan^{-1}\frac{\mathbb{I}\mathrm{m}\{t\}}{\mathbb{R}\mathrm{e}\{t\}}$ Unfortunately, computing Fourier Transform at each time-point t of a signal is tedious and computationally expensive. One approach to

address this drawback is to replace Fourier Transform by Hilbert Transform.

$$H(u)(t) = \frac{1}{\pi} \int_{-\infty}^{+\infty} \frac{u(\tau)}{\tau - t} d\tau = \mathbb{R}\mathrm{e}\{t\} + j\, \mathbb{I}\mathrm{m}\{t\} \tag{2.2}$$

Here too, the phase $\phi(t)$ is obtained similarly as above. For a given time-varying EEG signal $x(t)$, we then obtain for a referred interval $0 \leq t \leq nT$, where T is sampling interval of the EEG signal, and n is an integer identifying the highest number of samples being used depending on the selected perception problem.

2.2.2 Phase Quantisation

Though the phase relationship between 2 brain lobe taking part in perceptional process are in phase-synchrony, yet show difference in phase. This type of problem arises because of presence of noise in the EEG signals due to physiological artifacts(like eye blinking and undesirable motor noise, parallel thoughts). The approach is to quantize the phase $\phi(t)$ into uniform levels to overcome the problem. Let $\hat{\phi}(t)$ be the quantized interval of , obtained by

$$\hat{\phi}(t) = \lfloor \frac{\phi(t)}{N} \rfloor \tag{2.3}$$

where $\lfloor . \rfloor$ denotes the results of integer division. The smaller the value of N, the larger is the quantized $\phi(t)(\hat{\phi}(t))$. at the cost of loss in phase information. Again, the larger the value of N, the $\hat{\phi}(t)$ is too small and finding similarity between $\phi(t)$ and $\hat{\phi}(t)$ is too small and finding similarity between $\hat{\phi_1}(t)$ and $\hat{\phi_2}(t)$ of 2 channels would be difficult. A moderate value of N=37 is chosen to have 10^o quantized interval for the phase range $[-180^o, 180^o]$. Two channels, having same $\hat{\phi}(t)$, i.e., $\hat{\phi_1}(t) = \hat{\phi_2}(t)$ are perused to have phase-synchrony. The definition of phase-synchrony for n channels also extends the definition of 2 channels.

2.2.3 Finding Topological Connectivity:

At time point $t + T$, let C7 has the highest activation and C_1, C_5, C_9, C_{11} and C_{13} have phase symmetry, then the signaling behavior between time t and $t + T$ is such that there is a central node corresponding to the electrode having the maximum activation, which is in turn connected to multiple nodes having phase synchrony among them.

A percentage degree of correct scores evaluation of directed areas in the graphs is computed by the following formulation. Let numbers of areas in a graph are mismatched with those in the e-LORETA produced graph, and then the percentage degree of graph mismatching is given by

$$\text{Percentage Score} = \frac{D - d}{D} \times 100 \tag{2.4}$$

Using the above score, we obtain Table II to determine relative performance of the proposed technique with existing one.

2.2.4 Granger Causality Test

Granger Causality test[7]-[8] is widely used to understand relationship between multiple time series components. When two time-series are tested for Granger's causality, it is checked whether the first series have a causal effect on the second series or vice versa. For example in our case, comparing the values of the P_3 and the Fp_1 nodes, we take the null hypothesis H0: P_3 do not Granger-cause Fp_1 and test it against the test parameters. We assume that P_3 would be the independent variable and Fp_1, the dependent variable. Granger causality test is a statistical concept of causality that is based on prediction. According to Granger causality, if the signal P_3, Granger-causes (or G-causes) a signal Fp_1, then past values of P_3 should contain information that helps predict the future values of Fp_1, above and

beyond the information contained in past values of Fp_1 alone. Its mathematical formulation is based on linear regression modeling of stochastic processes. One of the most important constraints for using the Granger causality is that the time series should be stationary i.e., one whose statistical properties such as the mean, variance and autocorrelation are all constant over time. However, in our case the EEG signals are not stationary and thus Granger causality test cannot be applied directly. We can check for the stationarity of the time series using the augmented Dickey–Fuller (ADF) test which tests the null hypothesis that a unit root is present in the time series.[11] An important constraint in the Granger Causality test(GCT) is that it is highly sensitive to the selection of lags, because when the number of lags is changed, the result of the test may also change. So, in our case, choose the lags are chosen based on the Akaike Information Criterion (AIC) criterion in order to take a decision in a more robust manner.

We are using the Vector Autoregression (VAR) [12]-[13] model which works best on AIC criterion and a significant model can be found to perform a more robust GCT. VAR are multivariate linear time series models which are used to detect the joint dynamics of multiple time series signals. The Akaike Information Criterion [14] - [15] is used to select the best model considering multiple number of parameters, the number of observations and the squared sum of errors. The AIC criterion is given as follows:

$$AIC = Nln(\frac{SS_{error}}{N}) + 2K \tag{2.5}$$

Where N = number of observations; K = (1 + number of parameters we have fit); SS_{error}= Sum of squares error for the model.

The causality for each electrode on all the others is compared to determine its effect and if its causal. Then it is checked whether the signal flow is unidirectional or bidirectional and in order to get these result, we use the method of testing of

hypothesis. We do this for each possible combination of electrode and thus get a total of $\binom{19}{2}$ results. Let the two time series values at the i^{th} and j^{th} electrodes be given as $x_i(t)$ and $x_j(t)$ respectively. It is said that variable $x_i(t)$ Granger-causes variable $x_j(t)$ if and only if lagged values of the combined effect of both the time series can predict more accurately than just lagged values of one time series on itself. The testing method is based on ordinary least squares (OLS) regressions and is done as follows.

1. The following equations are defined as follows:

$$x_i(t) = \alpha_0 + \sum_{m=0}^{n} \beta_{1,m} x_j(t-m) + e_{1,t},$$
$$x_j(t) = \alpha_1 + \sum_{m=0}^{n} \beta_{1,m} x_j(t-m) + \sum_{m=1}^{n} \gamma_m x_i(t-m) + e_t$$

   where $e_t, e_{1,t}$ are i.i.d. (independent and identically distributed) error terms, α_0 and α_1 are constants, $\beta_{1,m}, \beta_m$ and γ_m for m = 1...n are coefficients.

2. The sum of squared residuals of both equations are calculated as follows:

$$E_1 = \sum_{t=1}^{N} \hat{e}_{1,t}^2,$$
$$E_2 = \sum_{t=1}^{N} \hat{e}_t^2$$

3. We determine the test statistic as follows:

$$T = \frac{\frac{E_1 - E_2}{n}}{\frac{E_2}{N-2n-1}}$$

$$where\ N = \text{sample size and}$$

$$n = \text{number of lags.}$$

The test statistics has asymptotically $F(n, N-2n-1)$ distribution. Here, the p-value method is used as it is more robust and does not take the critical values into account. Now,

$$p = \frac{\bar{x} - \mu}{\frac{\sigma}{\sqrt{n}}},$$

$$where\ \bar{x} = \text{sample mean,}$$

$$\mu = \text{population mean,}$$

$$\sigma = \text{population standard deviation , and}$$

$$n = \text{number of samples.}$$

4. Considering the null hypothesis when there is no Granger causality:

$$H_0 : c_i = 0, i = 1...n \tag{2.6}$$

We test the validity of the the null hypothesis using the p-parameter and reject it if it exceeds a certain level of significance. Then we conclude that the variable $x_i(t)$ Granger causes the variable $x_j(t)$. For the purpose of proper statistical inference, all of the variables included in the regression must be stationary [16]. The coefficients will be biased if a deterministic

process like a time trend has an effect on the variables and thus, the further statistical inference will be incorrect.

2.3 EXPERIMENTS AND RESULTS

The experimental framework, steps and main results obtained from the software simulation are summarized here.

2.3.1 Experimental framework

Ten healthy volunteers with normal eyesight have participated in the said experiments. Among the 10 subjects, 8 are men and 2 are women in the age group 22-30 years. They are requested to sit on a comfortable chair in a rest condition without movement to eliminate possible contamination by movement-related artifacts. Three primary colors (Red, Green, and Blue) are used as the visual stimuli.

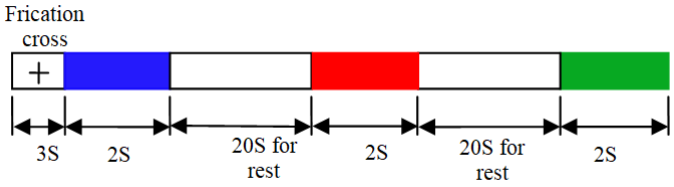

Figure 2.2: Presentation of Color Stimuli

Here we use 3 primary color(red,green and blue) as our visual stimuli. After fixation cross for 3 second, a random primary color is shown in the computer screen to the subject for 2 second. To avoid the distraction from environmental object color and the residual effect of the previous colored light, a time-gap of 20 second is maintained between two successive presentations of color stimuli in dark room. Each experiment with one colored stimulus presentation and EEG

recordings for one subject together constitutes one trial. Each trial is repeated 10 times over each subject. The sequence of presentation of the colored light was randomly selected in each trial from the list: red, green and blue. Figure 2.2 illustrates one sequence of color stimuli.

2.3.2 EEG data acquisition

Experiments are conducted using a standard 21 channels Nihon Kohden EEG data acquisition system having a sampling rate of 500 Hz to capture the EEG signals from the scalp of the subjects with the help of Ag/AgCl electrodes [16]. The electrodes are placed at the Fp1, Fp2, F3, F4, F7, F8, C3, C4, P3, P4, O1, O2, T3, T4, T5, T6, Fz, Cz and Pz locations according to the international 10/20 system for EEG recording [17]. The Fpz electrode is used as the ground and two earlobe electrodes A1 and A2 are used as the references for the right- and the left-side electrodes respectively. Figure 2.3(a) and (b) Present the experimental set up of colored stimuli.

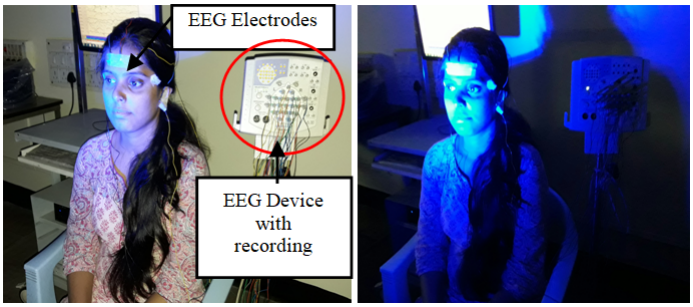

Figure 2.3: (a). Experimental set up during EEG signal acquisition from the scalp of subject . (b) Blue light projection on subject's eyes in dark environment,

2.3.3 EEG Pre-processing and artifacts removal

It is known that optical stimulation has the best brain response at the alpha lower band (8-10 Hz) and theta higher band (6-8 Hz) [17]. This inspired us to filter the acquired EEG using an active band pass filter of pass band = (6-10) Hz. Although there exist varieties of digital filter algorithms, we prefer elliptic filter

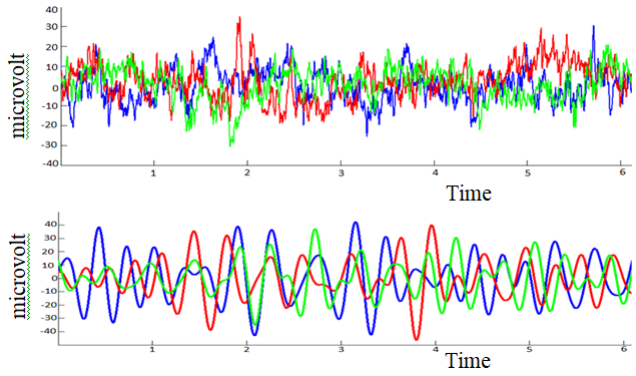

Figure 2.4: (a) Represent the raw EEG signal of Occipital lobe during three basic color light (Red, Green and Blue), (b) filtered data of three colored light

of order 10 for its smooth round-off characteristics around the cut-off frequencies. Figure 2. 4 provides the results of illustrative filter output

2.3.4 Phase Cluster for a particular time point

Results of phase clustering are shown in Figure 2.5. Here, the double circled nodes represent the electrode with the highest activation. Single circles represent lobes represent lobes having phase-synchrony with double circled lobes. The first four figures in Figure 1.5 are explained in detail in Table-I. Other figures are not included in the Table for space limitation.

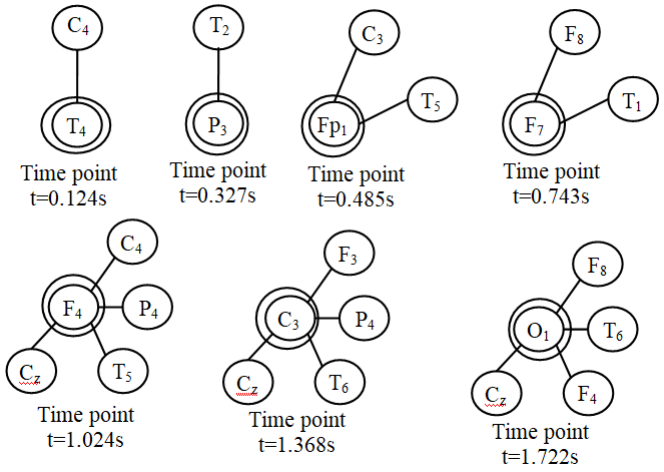

Figure 2.5: Interconnection between multiple channels for various time points of red color light using phase synchrony analysis

TABLE-I
ACTIVATION VALUES OF ELECTRODES WITH ACTIVATION TIME AND ELECTRODES IN PHASE-SYNCHRONY

Electrode position	Time of activation	Activation value	Electrodes in phase-synchrony with
T_4	0.124 s	0.00869574	C_4
P_3	0.327 s	0.00755436	T_2
Fp_1	0.485 s	0.00788545	C_3, T_5
F_7	0.743 s	0.00958412	F_8, T_1

2.3.5 Determine directionality between channels using Granger Causality test

After Granger causality test (GCT) is finished, the directed graph obtained as a response to the red and green color are shown in Figure 2.6,2.7 respectively. We

can see that different graphs are obtained for distinct colors (red and green).

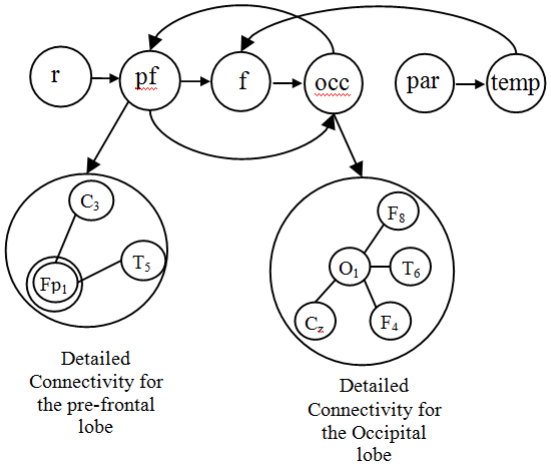

Figure 2.6: Directed graph for Red stimuli

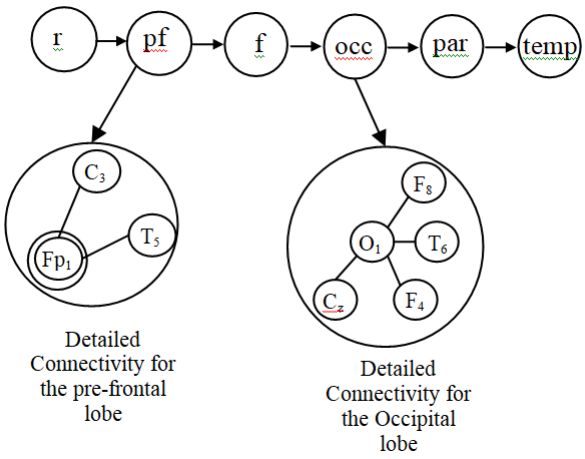

Figure 2.7: Directed graph for Green stimuli

From the output of the GCT, we get a causality matrix as depicted in Figure 2.8,2.9 and 2.10. Each cell in the matrix corresponds to the dependent electrode (rows) and the independent electrode (columns). In the given matrix, the purple colour indicates the causal electrodes, whereas the non-causal ones are denoted by yellow. If an electrode is causal with respect to another electrode , then the two electrodes are bidirectional for a given matrix. This causality test is performed

for each combination of two electrodes, and then the graph is plotted.

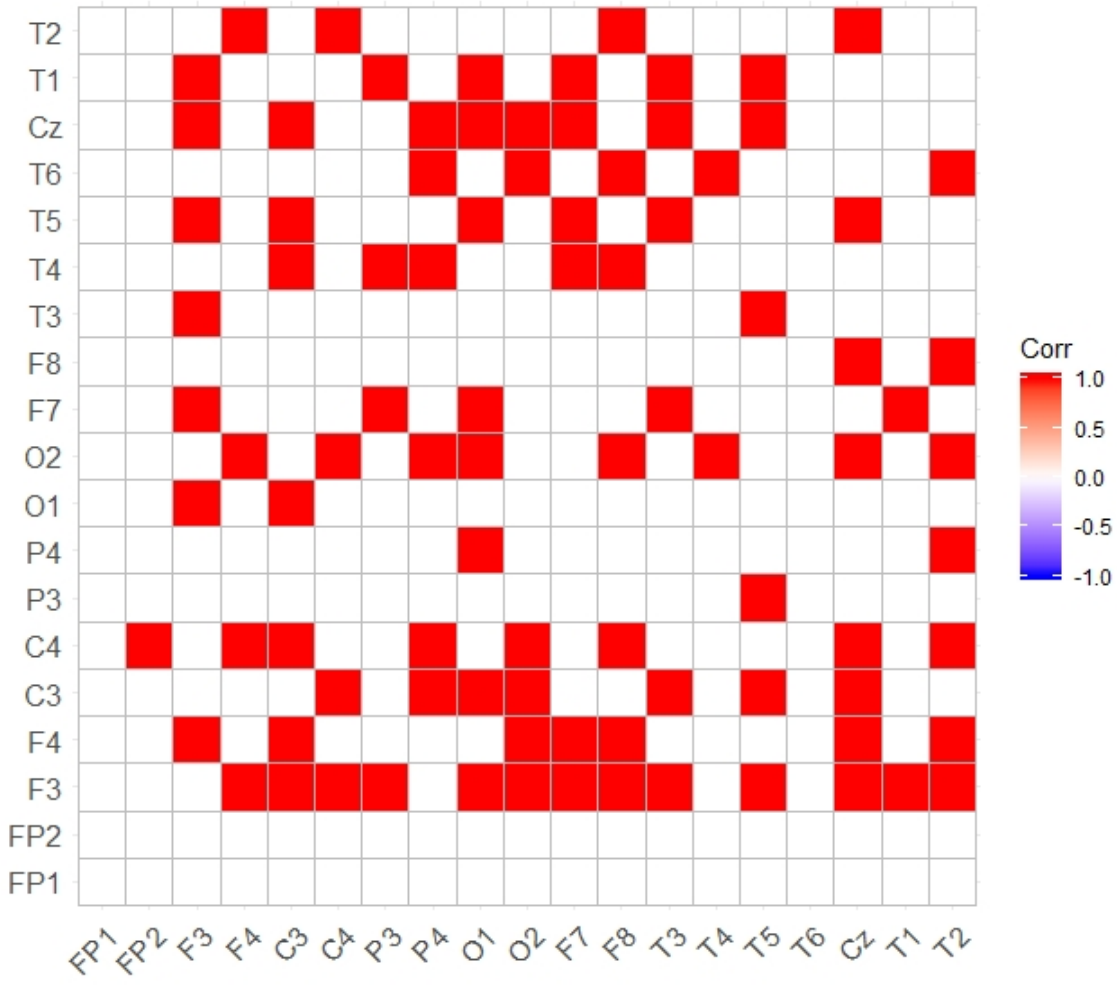

Figure 2.8: Output after obtaining causality matrix performing GCT for Red color

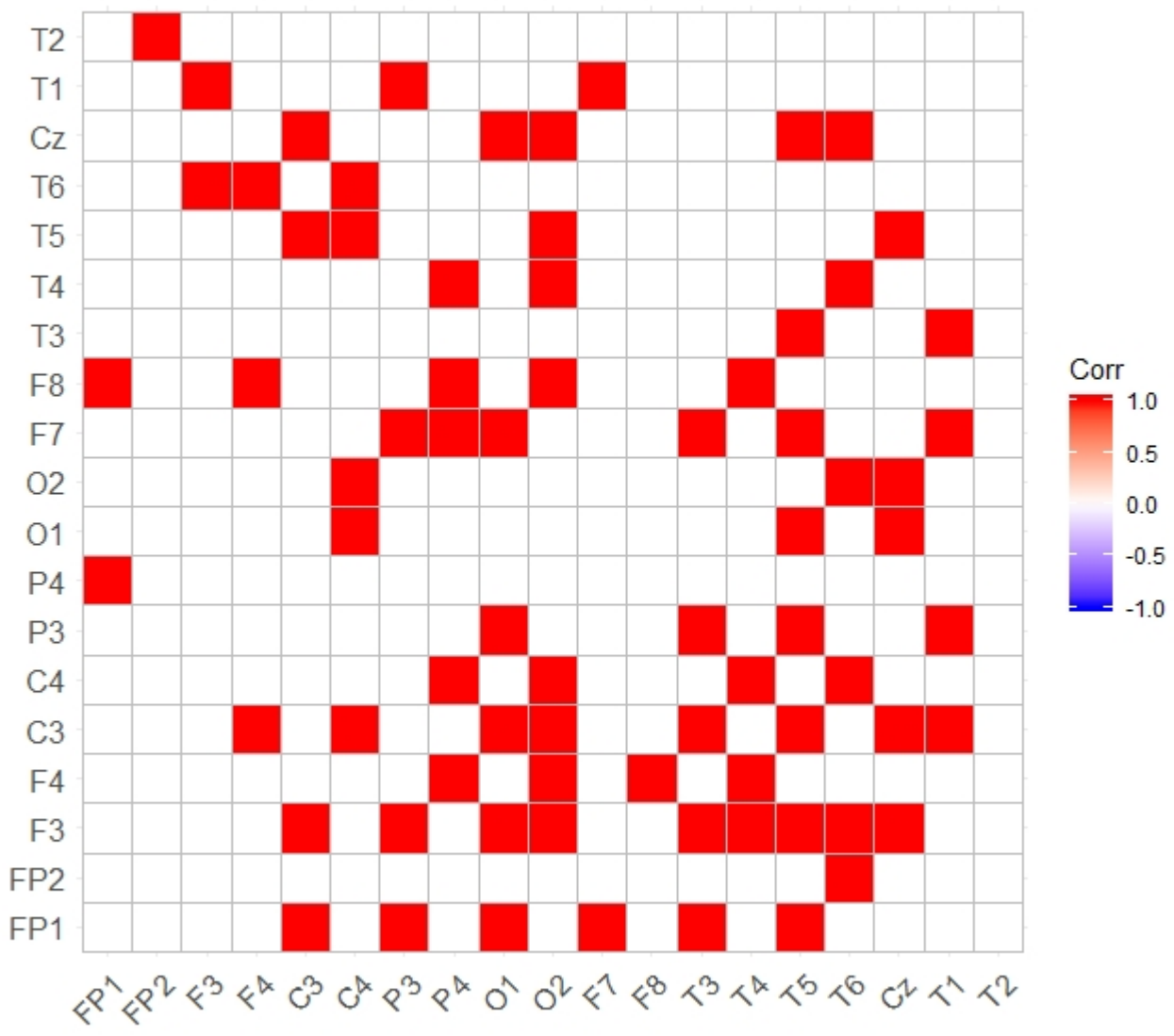

Figure 2.9: Output after obtaining causality matrix performing GCT for Green color

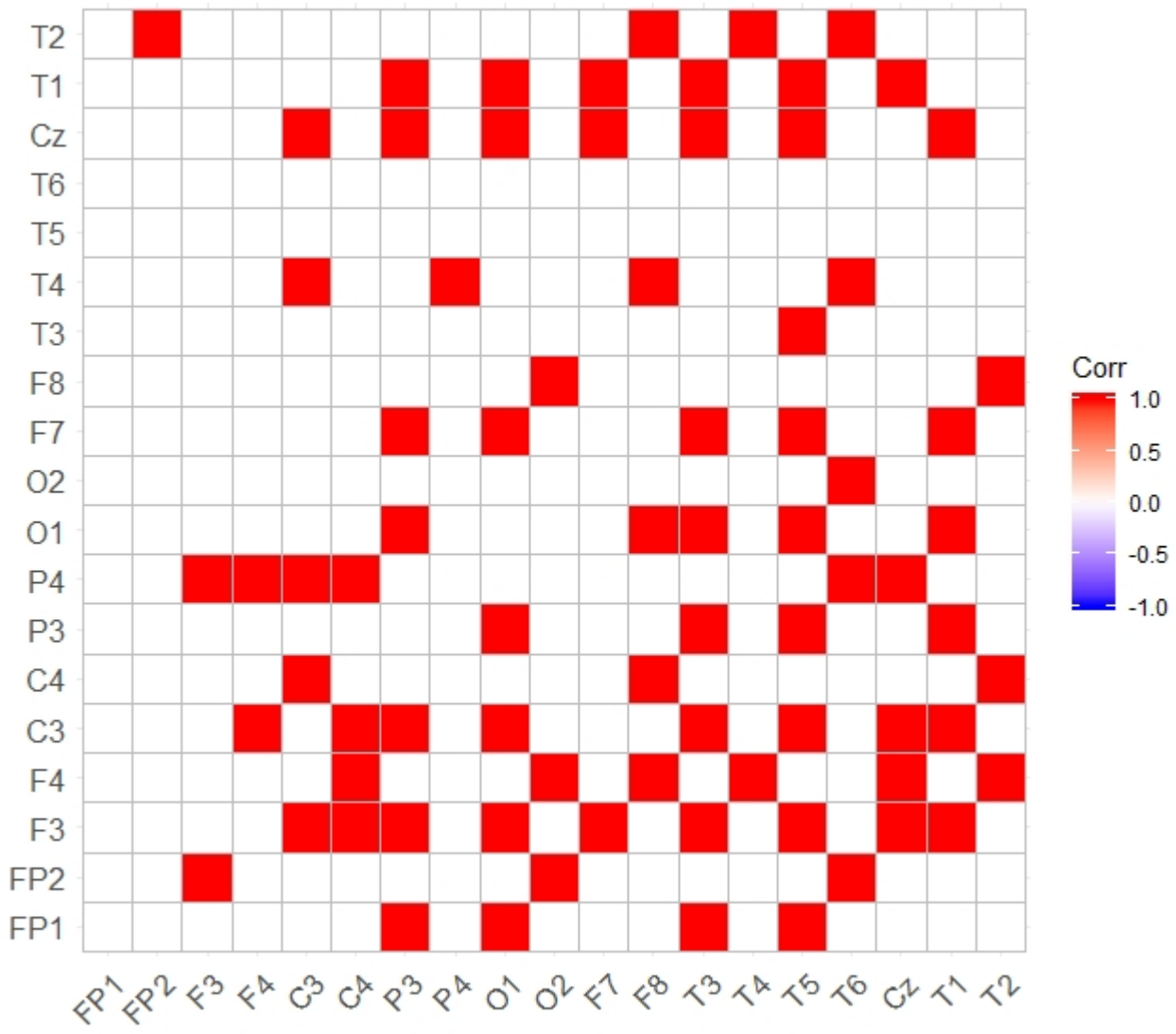

Figure 2.10: Output after obtaining causality matrix performing GCT for Blue color

Thereafter, the causality matrix obtained by this method is combined with the phase clusters obtained by the phase synchrony method

All the computation of GCT are done in Rstudio, a software for R programming. The required package for this GCT test are "VARS" and "tseries", which need to be installed from CRAN. It is already known that GCT is only applicable for stationary time series data, so first we need to check that the signal we are getting from each electrode are stationary or not. To do so, ADF test takes place to check the null hypothesis. We can say that a signal is stationary if we get p-value less than 0.05, by rejecting the null hypothesis of ADF test. In Figure 2.11 its shown that p-value of electrode "Fp1" is 0.211 which is larger than 0.05. so this is a non stationary data

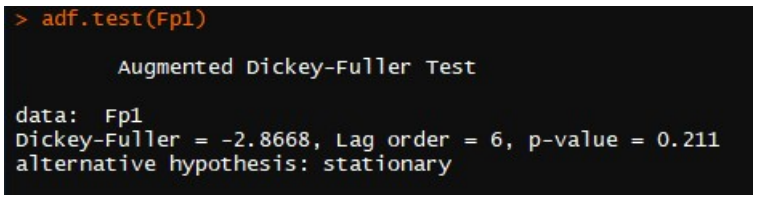

Figure 2.11: ADF test for a non-stationary signal

Then we are taking the first difference of the signal from "Fp1", and check again if it's stationary or not. We can see from the Figure 2.12 is that we get p-value less than 0.5, so it can be said that it is now a stationary time series data.

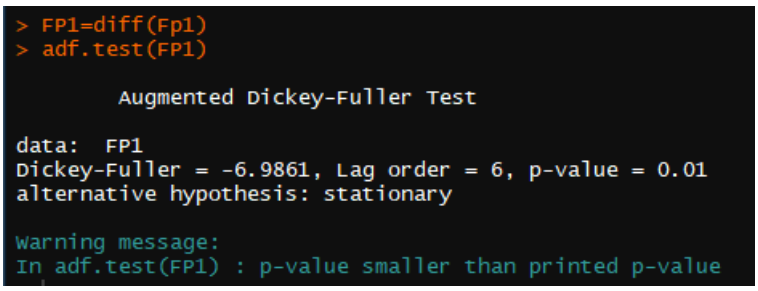

Figure 2.12: ADF test for a stationary signal

We repeat above two steps for each electrode to make the non stationary data, into stationary, so that we can proceed for GCT. VAR automatically choose the optimum lag value using AIC. Thus it's easy to check the causality between 2 electrode using VAR model. To compute the GCT between 2 time series signals, we check the causality for each one. Figure 2.13 shows that only "F3" G-causes "Fp1" by rejecting the null hypothesis: F3 does not Granger-causes Fp1. So, we can say that the causality between these 2 electrode is not bidirectional.

```
> p=causality((VAR((cbind(FP1,F3)),type="const",lag.max=10, ic="AIC")), cause="F3")$Granger
> p

        Granger causality H0: F3 do not Granger-cause FP1

data:  VAR object (VAR((cbind(FP1, F3)), type = "const", lag.max = 10, ic = "AIC"))
F-Test = 2.3157, df1 = 10, df2 = 536, p-value = 0.01135

> p=causality((VAR((cbind(FP1,F3)),type="const",lag.max=10, ic="AIC")), cause="FP1")$Granger
>
> p

        Granger causality H0: FP1 do not Granger-cause F3

data:  VAR object (VAR((cbind(FP1, F3)), type = "const", lag.max = 10, ic = "AIC"))
F-Test = 1.3043, df1 = 10, df2 = 536, p-value = 0.2246
```

Figure 2.13: GCT for 2 variable FP1 and F3

2.3.6 Performance Analysis

This experiment attempts to measure the percentage score for 3 basic colors for undirected and directed pathways realized by 2 approaches each. From the experimental results it is apparent in Table-II, that the proposed phase-synchrony followed by Granger causality method yields better performance than the rest with respect to percentage error metric.

TABLE-II
COMPARISON OF THE PERCENTAGE SCORES WITH THE EXISTING METHODS

Color stimulus	Undirected Pathway		Directed Pathway	
	Cross-correlation technique	**Phase-Synchrony technique**	Transfer entropy	**Granger Causality**
Red	75%	**90%**	86%	**95%**
Green	83%	**91%**	87%	**94%**
Blue	85%	**92%**	85%	**93%**

2.4 Conclusions

This chapter attempts to offer an interesting and useful solution to the well-known problem of determining signal transduction pathways among the brain lobes during color perception. A phase-synchrony method is employed to determine the brain lobes having common phase relationships. To determine the directed pathways in the graphs previously obtained by phase-synchrony analysis, a Granger causality based analysis is undertaken. Experiments results confirm that for 3 basic colors, the signal transduction pathways are different. A comparative study analyis confirms the results obtained by the proposed approach outperforms with respect to a defined percentage score than the other reported approaches.

References

[1] E. H. Land, "Recent advances in retinex theory and some implications for cortical computations: color vision and the natural image.," *Proceedings of the National Academy of Sciences of the United States of America*, vol. 80, no. 16, p. 5163, 1983. 24

[2] S. Zeki and L. Marini, "Three cortical stages of colour processing in the human brain.," *Brain: a journal of neurology*, vol. 121, no. 9, pp. 1669–1685, 1998. 24

[3] C. Cajochen, "Alerting effects of light," *Sleep medicine reviews*, vol. 11, no. 6, pp. 453–464, 2007. 24

[4] M. J. Goard, G. N. Pho, J. Woodson, and M. Sur, "Distinct roles of visual, parietal, and frontal motor cortices in memory-guided sensorimotor decisions," *Elife*, vol. 5, p. e13764, 2016. 24

[5] F. Varela, J.-P. Lachaux, E. Rodriguez, and J. Martinerie, "The brainweb: phase synchronization and large-scale integration," *Nature reviews neuroscience*, vol. 2, no. 4, p. 229, 2001. 24

[6] F. Mormann, K. Lehnertz, P. David, and C. E. Elger, "Mean phase coherence as a measure for phase synchronization and its application to the eeg of epilepsy patients," *Physica D: Nonlinear Phenomena*, vol. 144, no. 3-4, pp. 358–369, 2000. 24

[7] M. Droumaguet, A. Warne, and T. Woźniak, "Granger causality and regime inference in markov switching var models with bayesian methods," *Journal of Applied Econometrics*, vol. 32, no. 4, pp. 802–818, 2017. 24, 25, 28

[8] A. Roebroeck, E. Formisano, and R. Goebel, "Mapping directed influence over the brain using granger causality and fmri," *Neuroimage*, vol. 25, no. 1, pp. 230–242, 2005. 24, 25, 28

[9] M. Lobier, F. Siebenhühner, S. Palva, and J. M. Palva, "Phase transfer entropy: a novel phase-based measure for directed connectivity in networks coupled by oscillatory interactions," *Neuroimage*, vol. 85, pp. 853–872, 2014. 25

[10] S. Siuly and Y. Li, "Improving the separability of motor imagery eeg signals using a cross correlation-based least square support vector machine for brain–computer interface," *IEEE Transactions on Neural Systems and Rehabilitation Engineering*, vol. 20, no. 4, pp. 526–538, 2012. 25

[11] F. Varela, J.-P. Lachaux, E. Rodriguez, and J. Martinerie, "The brainweb: phase synchronization and large-scale integration," *Nature reviews neuroscience*, vol. 2, no. 4, p. 229, 2001. 29

[12] U. Triacca, "A pitfall in using the characterization of granger non-causality in vector autoregressive models," *Econometrics*, vol. 3, no. 2, pp. 233–239, 2015. 29

[13] H. Y. Toda and P. C. Phillips, "Vector autoregression and causality: a theoretical overview and simulation study," *Econometric reviews*, vol. 13, no. 2, pp. 259–285, 1994. 29

[14] Y. Sakamoto, M. Ishiguro, and G. Kitagawa, "Akaike information criterion statistics," *Dordrecht, The Netherlands: D. Reidel*, vol. 81, 1986. 29

[15] K. J. Blinowska, R. Kuś, and M. Kamiński, "Granger causality and information flow in multivariate processes," *Physical Review E*, vol. 70, no. 5, p. 050902, 2004. 29

[16] R. K. Green, "Follow the leader: how changes in residential and non-residential investment predict changes in gdp," *Real Estate Economics*, vol. 25, no. 2, pp. 253–270, 1997. 31

[17] A. Yoto, T. Katsuura, K. Iwanaga, and Y. Shimomura, "Effects of object color stimuli on human brain activities in perception and attention referred to eeg alpha band response," *Journal of Physiological Anthropology*, vol. 26, no. 3, pp. 373–379, 2007. 34

Chapter 3

Brain Connectivity Analysis in Color-Perception Problem Using Convergent Cross Mapping Technique

Abstract

Traditionally, Granger Causality analysis is employed to handle the problem. However, due to the applicability of Granger Causality analysis for purely stochastic systems only, its suitability of applications in brain-connectivity analysis is limited due to the presence of both deterministic and stochastic characteristics in the human brain. Additionally, because of high parameter sensitivity of Granger Causality technique, identifying the right set of parameters itself poses an additional problem. Convergent cross mapping overcomes the above limitations and thus has immense scope for exploitation in brain-connectivity analysis. Here, we make an honest attempt to determine brain-connectivity during

subjective engagement in color perception using convergent cross mapping technique. Experimental results envisage that the proposed technique yields precise brain-connectivity in color percerption in comparison to those obtained by the state-of-the-art techniques.

3.1 Introduction

The human brain comprises several billions of neurons, distributed in the cortex. A cognitive task, such as perception, reasoning, learning, planning, etc., involves several clusters of neurons distributed across the brain. These clusters lie on the signal transduction pathways of the brain to successfully execute the cognitive task. Color-perception is an important cognitive task, aiming at understanding the structure/geometry of objects based on their color content. When colored light reflected by a colored object is incident on the retina of the human eye, the cone cells present in the retina get excited, resulting in electrical signals. These signals are carried by the optic nerves terminated at the retina to different cortical regions for understanding and recognition of the colored object. The motivation of the present research is to detect the brain-connectivity on the signalling pathways when the brain is engaged in color-perception.

One approach to experimentally determine brain-connectivity is to identify the causal dependence of the temporal signals acquired from different electrodes mounted over the scalp. Electroencephalography (EEG) provides the temporal activations of the local neurons in a brain lobe, and this can be used as the primary resource for the present study. There exists quite a few interesting techniques to determine the causal relationship between pairs of time-varying signals. A few of these that need special mention include Granger Causality [1][2] analysis, Probabilistic Relative Correlation Adjacency Matrix (PRCAM)[3], transfer entropy [4],

and the most recent one, called convergent cross mapping [5]. Although, extensive works on Granger Causality based analysis in determining brain-connectivity are available in the literature [6] [2], the results reported are not free from errors for the following reasons. First, Granger Causality analysis is restrictive to linear prediction model and thus may not be convenient to predict non-linear mapping between pairs of time-varying brain signals. Further, Granger Causality is only applicable for stationary time series. Thus, it might result in errors when applied directly to non-stationary EEG signals without considering local stationarity. Lastly, because of high parametric sensitivity of the Granger Causality model, it is often difficult to rightly select the optimal model parameters for the performance.

The above limitations inspired the author to take into account of an alternative technique to handle the same old problem. Convergent cross mapping (CCM) is fortunately free from the above limitations and has successfully been exploited in many time series causality analysis [7] [8] [9] [10].

The promising success of CCM inspired the author to explore its possibility in brain-connectivity analysis for subjective engagement in color-perception.

3.2 Principles and Methodology

This section aims at describing the Convergent Cross Mapping technique and how it has been used in the brain connectivity analysis for the color-perception problem in detail. The steps involved are as follows:

1. Acquire EEG data from healthy subjects with normal eyesight and no background of color blindness.

2. Select the active brain regions for a stimulus using the e-Loreta software.

3. Consider the EEG data from the activated brain regions as obtained by eLoreta.

4. Apply necessary filtering and pre-processing procedures on the selected EEG data from the previous step for noise and artefact removal.

5. Apply Convergent Cross Mapping algorithm on the filtered EEG time series.

6. From the directed causality matrices obtained from CCM calculations, apply graph theory analysis to obtain effective information pathways in the brain.

The experimental workflow is illustrated in Fig. 3.1.

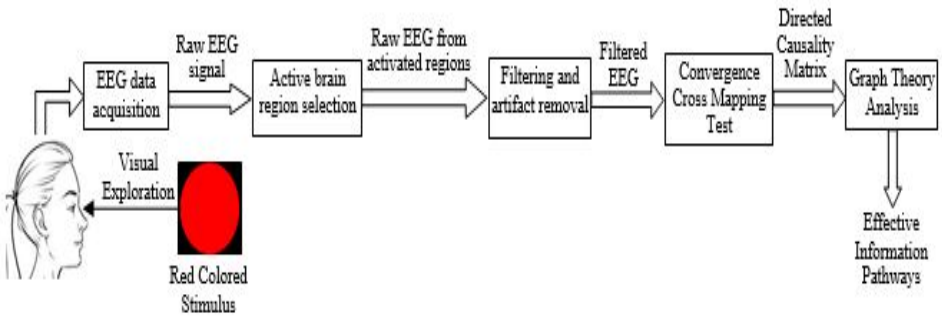

Figure 3.1: Block Diagram of Overall System

3.2.1 Convergent Cross Mapping

Convergent Cross Mapping (CCM)[5] is a recent technique used to determine the cause-and-effect relationship between two time series variables. It seeks to resolve the old problem "***Causation does not imply correlation***", i.e., the presence of correlation between two variables does not always necessarily mean there exists

a causal relationship between them, and vice-versa. Granger Causality, which is another statistical causality testing technique, relies on the key requirement of separability [5]. CCM, on the other hand, works on the principle of reconstructing system states from two time series variables using predetermined parameters, and then quantifying the relationship between them using a nearest neighbor algorithm.

The ideas for CCM were developed following time-delay embedding theorems, most notably from Takens' Theorem [15]. As described by Takens[15], an attractor manifold can be reconstructed from a set of observation variables of a dynamical system. This reconstruction preserves not only the properties of the dynamical system but also the topological structure of the original attractor. In order to explain CCM, some practical example is going to be discussed here. We need recent version of R and rEDM package for this activities. Rstudio is an open source software for R programming where we can easily install rEDM package. First, consider two discrete time series variables *X(t)* and *Y(t)*, where t denotes time, of length L (library length) from a dynamical system having a common attractor manifold, M. Now simulate *X(t)* and *Y(t)* to create a dynamical time series data of length 150 and plot both of these.

```
library(rEDM)
## Two vectors to store data
X <- c()
Y <- c()
## Initial values
X[1] <- 0.1
Y[1] <- 0.1
## Iterate the dynamics 150 time steps
for(i in 2:150){
X[i] <- X[i-1]*(3.77*(1-X[i-1]))
Y[i] <- Y[i-1]*(3.82*(1-Y[i-1])-0.32*X[i-1])
}
XY<-as.data.frame(cbind(X,Y))
#plot both time series in a single graph
plot(20:60,X[20:60],type="b", pch=18, col="blue",ylim=c(0,1), main='Two Species',xlab = 'time',ylab='
     Population')
lines(20:60,Y[20:60],pch=19, col="red", type="b",lty=2,lwd=2)
legend(x = "bottomright", legend = c("X(t)", "Y(t)"),lty=c(1,2), col = c("blue", "red"), inset = 0.02,lwd
     =2)
```

Fig. 1 illustrate the example time series given by

$$\begin{cases} X(t) = X(t-1)[3.77 - 3.77X(t-1)] \\ Y(t) = Y(t-1)[3.82 - 3.82Y(t-1) - 0.32X(t-1)] \end{cases}$$

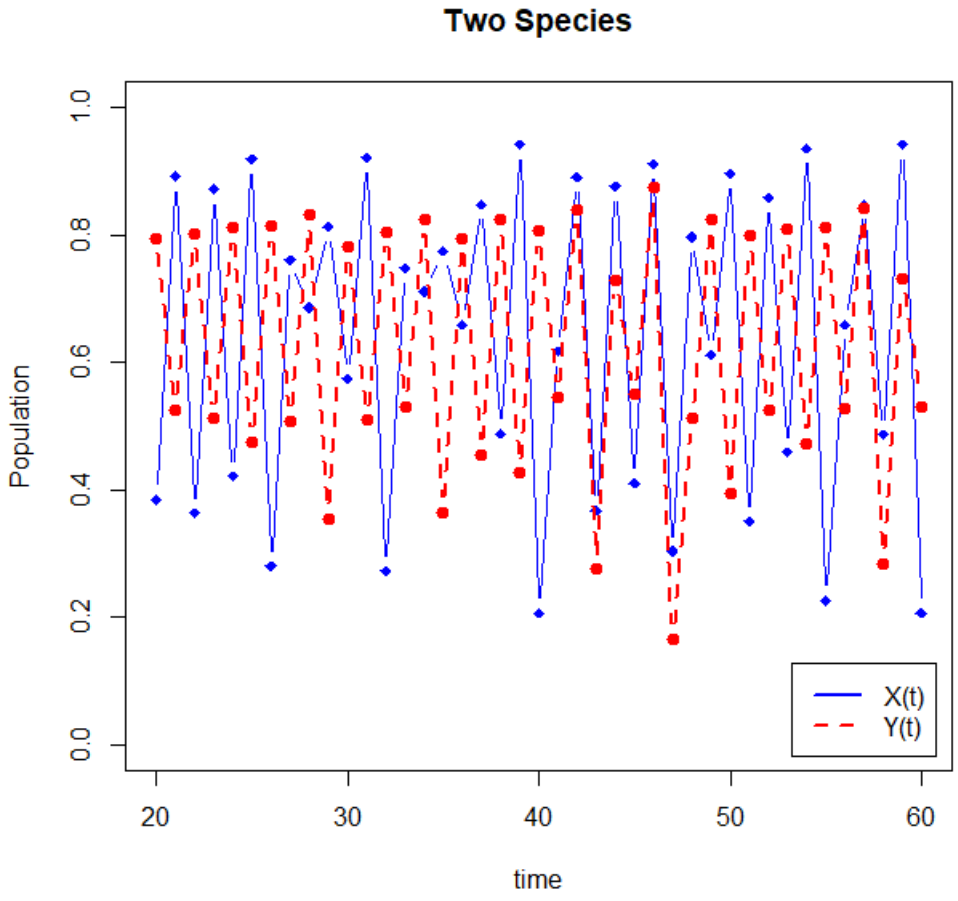

Figure 3.2: Time series X(t) and Y(t)

From the above plot we can not decide whether these 2 time series are correlated or not, although from the equation we can say that values of X(t) is causing changes in Y(t) Using Takens' time-delay embedding theorem, E-dimensional shadow manifolds M_X and M_Y, with successive delayed time steps τ, can be constructed for time series *X(t)* and *Y(t)* respectively, where E is the embed-

ding dimension. The shadow manifold M_X can be represented as: $\underline{x}(t) = <X(t), X(t-\tau), X(t-2\tau), ..., X(t-(E-1)\tau)>$, where τ is positive, and $\underline{x}(t)$ are the points on the shadow manifold M_X. Generally, points on M_X has a one-to-one correspondence to the original manifold M[5]. M_Y can be constructed similarly. Next, CCM aims to discover the degree of correspondence between the local neighborhoods of M_X and M_Y [5] . Coincidental values of $X(t)$ can be estimated from the shadow manifold M_Y, and vice-versa.

We first need to find the optimal E for both X(t) and Y(t) by Simplex Projection [**?**] to construct the manifold.

```
simplex_X<-simplex(X,silent=T)
plot(simplex_X$rho,type='o', ylab = "Forecast Skill (rho)", xlab="Embedding Dimension (E)")
#find the Embded dimention for maximum forcasting skill of X(t)
E_X<-which.max(simplex_X$rho)
E_X
[1] 2
simplex_Y<-simplex(Y,silent=T)
plot(simplex_Y$rho,type='o', ylab = "Forecast Skill (rho)", xlab="Embedding Dimension (E)")
#find the Embded dimention for maximum forcasting skill of Y(t)
E_Y<-which.max(simplex_Y$rho)
E_Y
[1] 2
```

The optimal embedding dimension (E) is 2 for both X(t) and Y(t), because for E=2, we get the largest prediction skill ρ. As we know the E for both the time series, now we can proceed to construct the manifold M_x and M_Y using the make-block function from rEDM package.

```
# max_lag is the optimal embedding dimension
Shadow_MXY<-make_block(XY,max_lag = 2)
Shadow_MX<-Shadow_MXY[,2:3]
Shadow_MY<-Shadow_MXY[,4:5]
head(Shadow_MXY)
time          X       X_1          Y       Y_1
  1     0.1000000        NA 0.1000000        NA
  2     0.3393000 0.1000000 0.3406000 0.1000000
  3     0.8451417 0.3393000 0.8209591 0.3406000
  4   0.4934071 0.8451417 0.3394592 0.8209591
  5   0.9423361 0.4934071 0.8029485 0.3394592
  6     0.2048571 0.9423361 0.3622817 0.8029485
```

From the above table we know that M_x is constructed by X and X_1, and M_Y is constructed by Y and Y_1.

For better understanding, start predicting a single value in Y by using the X. Here instead of predicting the value of X from its past dynamics, we are performing "cross-prediction" between different variable but for the same time point. Let we want to predict the value $Y(t = 18)$, so to predict this, a nearest-neighbor algorithm can be employed by considering *E+1* nearest neighbors. The number of nearest neighbors can be chosen using the relation $k \geq E+1$, where k denotes the number of nearest neighbors. We are going to use nearest neighbor of $X(t = 18)$ within M_x. Next, the time indices (from closest to farthest) of the *E+1* nearest neighbors to $\underline{x}(t)$ on M_X are indicated by t_1, ..., t_{E+1}.

```
predictor<-18
print(Y[predictor])
[1] 0.826084
dist.matrix_X <- as.matrix(dist(Shadow_MX, upper=TRUE))
neigb_X <- order(dist.matrix_X[predictor,])[2:4]
neigh_X_print<-c(neigb_X)
print(paste('simplex_Mx:',list(neigh_X_print)))
[1] "simplex_Mx: c(150, 82, 49)"
```

Now we are going to plot M_x with predictor(blue dot) and their nearest neighbor(red dot). To estimate the value of $Y(t = 18)$, we find the point indexes in M_y, obtained by $simplex_M x$ and then plot these points on M_y. From these points we can predict Y, denoted by $\hat{Y}$. This idea of predicting a single point Y from X can be expand to predict the every value of Y from X. Then we can compare the original value of Y with the predicted one. The construction of cross mapping of $\hat{Y}(t)$ for *Y(t)* can be done with the help of these time indices by:

$$\hat{Y}(t)|M_X = \sum w_i Y(t_i)\,, \tag{1}$$

where, i=1, ..., E+1

and, w_i are the weights based on the distance of each E+1 nearest neighbors from $\underline{x}(t)$, $Y(t_i)$ are the coincidental values of $Y(t)$. The weights can be estimated by

$$w_i = \frac{u_i}{\sum u_j}, \tag{2}$$

where, $j = 1, ..., E+1$

$$u_i = e^{-\frac{d(\underline{x}(t), \underline{x}(t_i))}{d(\underline{x}(t), \underline{x}(t_1))}}, \tag{3}$$

where $d[a, b]$ is the Euclidean distance between vectors a and b. $\hat{X}(t)|M_Y$ can be estimated similarly.

```
plot(Shadow_MX, main="Mx", xlab='X(t)', ylab='X(t-1)')
points(Shadow_MX$X[predictor],Shadow_MX$X_1[predictor],col='blue',pch=16,cex=0.8)
points(Shadow_MX$X[neigh_X_print],Shadow_MX$X_1[neigh_X_print],col='red',pch=16,cex=0.8)
plot(Shadow_MY, main="My", xlab='Y(t)', ylab='Y(t-1)',cex=0.8)
points(Shadow_MY$Y[neigh_X_print],Shadow_MY$Y_1[neigh_X_print],col='red',pch=16,cex=0.8)
```

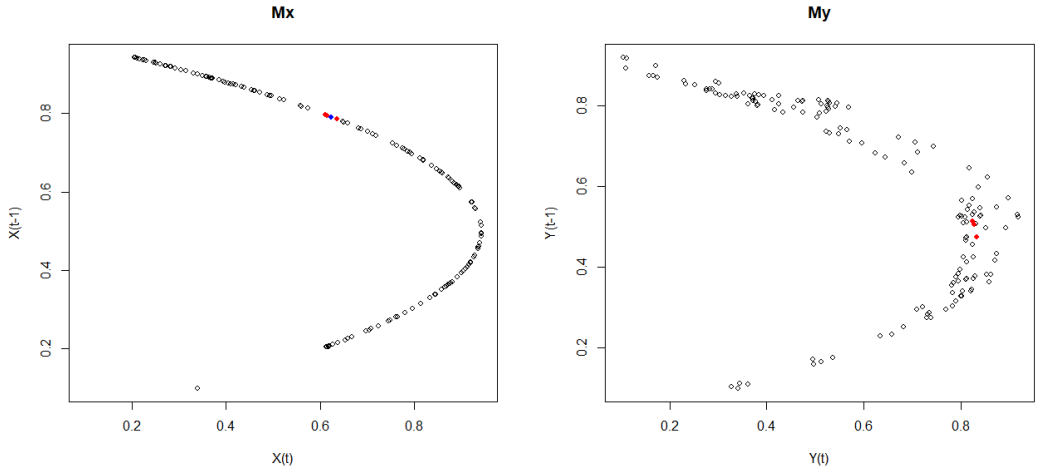

(a) Mx with Nearest neighbor of the value to be predicted on Y

(b) My with point indexes to predict the Y

Figure 3.3: shadow manifold Mx and My with predicted and nearest neighbor

```
lib <- c(1, NROW(Shadow_MXY))
block_lnlp_output_XY <- block_lnlp(Shadow_MXY, lib = lib, pred = lib, columns = c("X","X_1"), target_
    column = "Y", stats_only = FALSE, first_column_time = TRUE)
observed_all_Y <- block_lnlp_output_XY$model_output[[1]]$obs
predicted_all_Y <- block_lnlp_output_XY$model_output[[1]]$pred
pred_obs_Y<-as.data.frame(cbind(predicted_all_Y,observed_all_Y)) #
colnames(pred_obs_Y)<-c('Predicted Y','Observed Y')
head(pred_obs_Y)
  Predicted Y Observed Y
1         NaN  0.3406000
2   0.6523674  0.8209591
3   0.7839948  0.3394592
4   0.5290611  0.8029485
5   0.7693002  0.3622817
6   0.5725587  0.8587995
pred_obs_Y[(predictor-2),]
   Predicted Y Observed Y
16   0.4690784  0.4253729
```

All these above step can be repeated to predict the value of X from Y, then compare the cross map skill. The indicator of the cross map skill is quantified by Pearson's Correlation Coefficient [16](Eq. 4), ρ (rho), between the estimated $(\hat{Y}(t)|M_X)$ and observed values of $Y(t)$.

$$\rho = \frac{N\sum XY - (\sum X \sum Y)}{\sqrt{[N\sum x^2 - (\sum x)^2][N\sum y^2 - (\sum y)^2]}} \,. \tag{4}$$

The cross map skill ranges between 0 and 1. The causal relationship is judged by checking if the increasing library length dictates an increase in the cross mapping skill and converges it to a plateau.since all our data is synthetic, we know this is true: we created the variable X independently of Y, and X was causing changes in Y. So when X causes Y, the cross mapping skill from M_y to M_X ($Y_x map_X$) will generally gives us good results (high correlations), but not$X_x map_Y$. It is very important to notice that there is an inverse relation between cross mapping and causality: if X causes Y (X→Y), Y cross map of X ($Y_x map_X$) shows a positive (large) correlation. In practice, the cross map skill is checked over increasingly large library lengths and the optimal cross map estimation is taken at largest library length. The reason is that with increasing library length, the distances

between the E+1 nearest neighbors decreases as the attractor manifold fills in, thus resulting in higher correlation[5].This means that the more data you have (i.e. the larger L), the more trajectories you have to infer the attractor, resulting thus in closer nearest neighbors and less estimation error.

```
X_xmap_Y<- ccm(XY, E = 2, lib_column = "X", target_column = "Y",
lib_sizes = seq(10, 130, by = 10), num_samples = 100, random_libs = TRUE,
replace = TRUE)
# cross map from Y to X
Y_xmap_X<- ccm(XY, E = 2, lib_column = "Y", target_column = "X",
lib_sizes = seq(10, 130, by = 10), num_samples = 100, random_libs = TRUE,
replace = TRUE)

# mean values
X_xmap_Y_means <- ccm_means(X_xmap_Y)
Y_xmap_X_means <- ccm_means(Y_xmap_X)

# plot graphs
plot(X_xmap_Y_means$lib_size, pmax(0, X_xmap_Y_means$rho), type = "l", col = "red",
main='Two Species', xlab = "Library Size (L)",
ylab = "Cross Map Skill (Pearson rho)", ylim = c(0,1))
lines(Y_xmap_X_means$lib_size, pmax(0, Y_xmap_X_means$rho), col = "blue")
legend(x = "topleft", legend = c("X(t)_xmap_Y(t)", "Y(t)_xmap_X(t)"), col = c("red", "blue"),
cex=1.1,lwd=2, inset = 0.02)
```

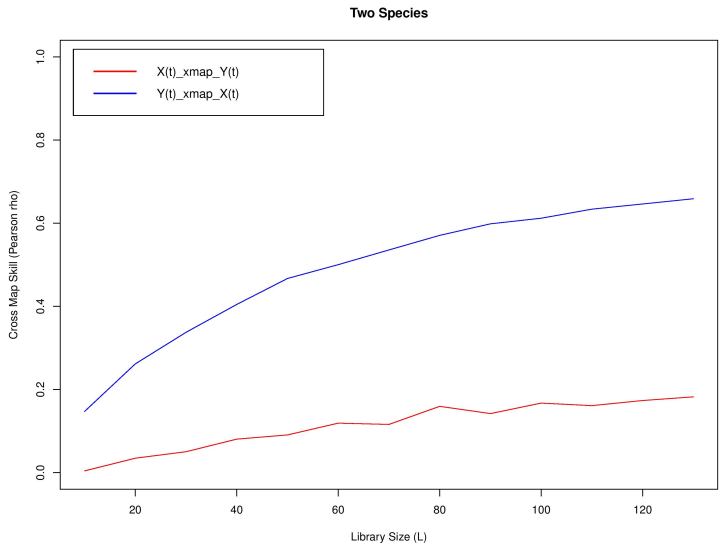

Figure 3.4: Cross mapping index between X(t) and Y(t) over increasing library lengths

The Convergent Cross Mapping algorithm for estimating $\hat{Y}(t)|M_X$ can be

summarized in the following steps:

1. Consider two time series variables *X(t)* and *Y(t)* of length L,
2. Reconstruct an E-dimensional shadow manifold M_X with successive delayed time steps τ (tau),
3. The values of parameters E and τ (tau) for a time series have been calculated following simplex projection [17], i.e., the value of the parameters are the ones that correspond to the values that best unfold the reconstructed attractor and give the highest forecasting (rho) (as shown in Fig. 3 for the experimental EEG data O_1),
4. Find E+1 nearest neighbors at each time index in M_X,
5. Create weight matrix by use of nearest neighbors,
6. Estimate $\hat{Y}(t)|M_X$ by use of weights,
7. Calculate correlation coefficient *rho* (ρ) between *Y(t)* and $\hat{Y}(t)|M_X$.

3.3 Experiments and Results

This section is covered with the whole experiment procedure, software simulation and result obtain from the software simulation.

3.3.1 Experimental Framework

The experiment has been performed in the Artificial Intelligence Laboratory at Jadavpur University. Ten healthy volunteers (6 male and 4 female) aged between 24 $\pm$ 2 years with normal eyesight and no background of color blindness have

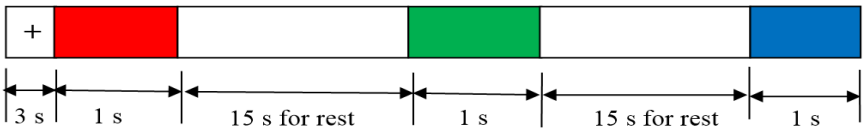

Figure 3.5: Presentation of Color Stimuli

participated in the experiments. The primary colors (Red, Green, and Blue) are used as visual stimuli.

For the light source, we used 15W RGB remote controlled bulbs connected with a 110-220 V power source supply. In accordance with the pre-tested tolerance levels of the subjects, the light sources are kept at a maximum intensity level. Each subject is continuously exposed to one of the primary coloured lights for 1 seconds. The subject is then asked to take a rest for 15 seconds in order to avoid the residual effect of the previous colored light. The structure of stimulus with timing details is depicted in Fig.3.5. A single trial comprises of the presentation of one colored stimulus and acquisition of EEG data for one subject. Each trial is repeated over one subject for 10 times. The sequence of the colored stimulus being presented in each trial was randomly selected.

3.3.2 Preparing the Data set for Color Perception

The experiments are conducted using a stand-alone 32 channel Nihon Kohden EEG data acquisition system to capture the EEG signals from the scalp of the subjects with the help of Ag/AgCl electrodes. The electrodes are placed at the Fp_1, Fp_2, F_3, F_4, O_1, O_2, F_7, F_8, T_7, T_8, P_7, P_8, FT_9, and FT_{10} locations in accordance to the standard 10/20 electrode placement system. The sampling frequency of the recording was set at 500 Hz.

Due to the high computational cost of the Convergent Cross Mapping (CCM) procedure and to reduce the processing time, the EEG data are down-sampled

from 500 Hz to 250 Hz, thereby resulting in a reduction of the trial length by half.

3.3.3 Active Brain Region Selection Using e-LORETA

In this experiment, we evaluate the electrical activity of the intra-cortical distribution obtained from the EEG data using e-LORETA software [11] [12] [13]. To determine the highly active brain regions for three different color stimuli, we use linear inverse solution technique. As mentioned above, the total experimental duration for color stimulus is one second (1×1000=1000 milliseconds). The entire sample values, obtained during 1 seconds, are divided into 10 time frames in the e-LORETA software. Thus, the brain activation in each time-frame of duration 0.01 seconds (100 milliseconds), evaluated by the e-LORETA software is observed carefully. According to the activation values of different time frames, we observe that occipital, pre-frontal, frontal and temporal lobes have higher activation than the remaining ones for all the three colors. The highest activation regions for red, green, and blue color perception, obtained by e-LORETA, are depicted in Fig.3.6(a) to (c).

3.3.4 Data Pre-processing and Artefact Removal

The EEG signal obtained from the highest activity regions (occipital, pre-frontal, frontal and temporal) are then passed through various signal pre-processing steps to remove the noise or artefacts, that are crept into the signal due to ocular and involuntary muscular activation. The signals are first band pass filtered using an Infinite Impulse Response (IIR) Elliptical band pass filter of order 10 and of suitable pass and stop band frequencies. To select the required frequency bandwidth of the filter, Fourier transform of the EEG signals is performed. It is found that the highest amplitudes of the Fourier spectra for all the three basic colors

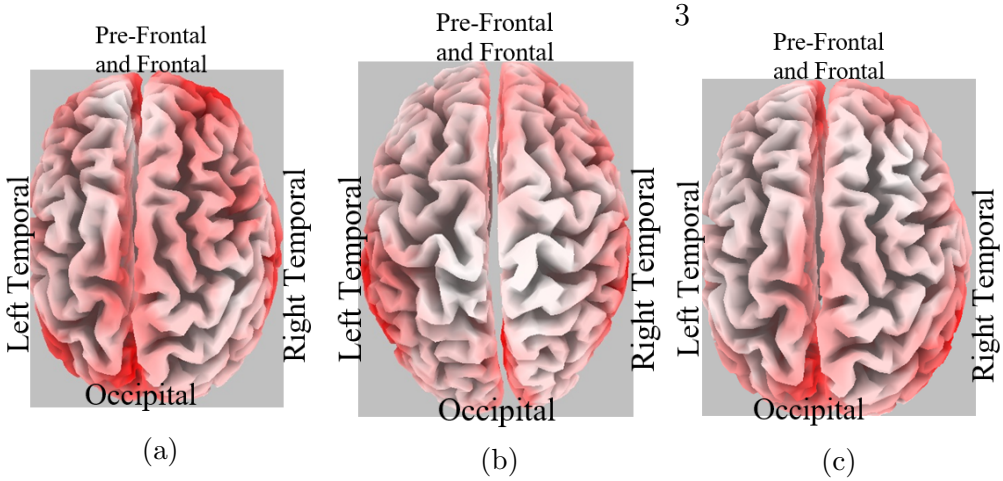

Figure 3.6: eLORETA solutions for (a) red color, (b) green color and (c) blue color stimuli

(red, blue and green) lie between 5 and 15 Hz. Therefore, the bandwidth of the filter is chosen as 5 to 15 Hz. The band pass filtered EEG signals are then further pre-processed using Independent Component Analysis (ICA) [14] to remove the eye-blinking and muscular artefacts.

3.3.5 Effective Connectivity Estimation by CCM Algorithm

To get the effective connectivity for this color perception problem, first check the causality between the electrode by CCM method. To do so, shadow manifold of each electrode is reconstructed by computing the optimum Embedding dimension(E) and time delay(τ) by simplex projection. Hence from the reconstructed manifold we check the cross map skill for every possible combination of electrode pair.

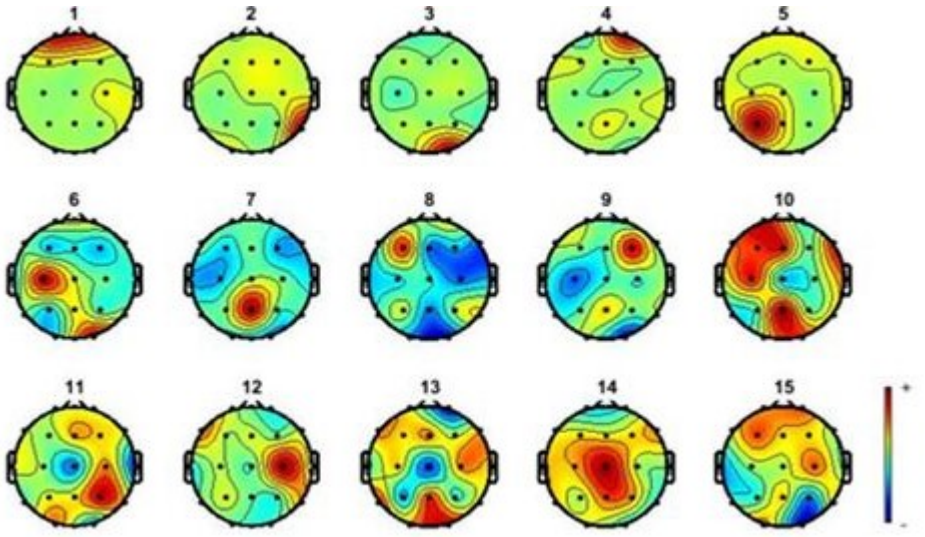

Figure 3.7: 2D topographical maps for red color stimulus obtained using ICA from EEGLAB toolbox

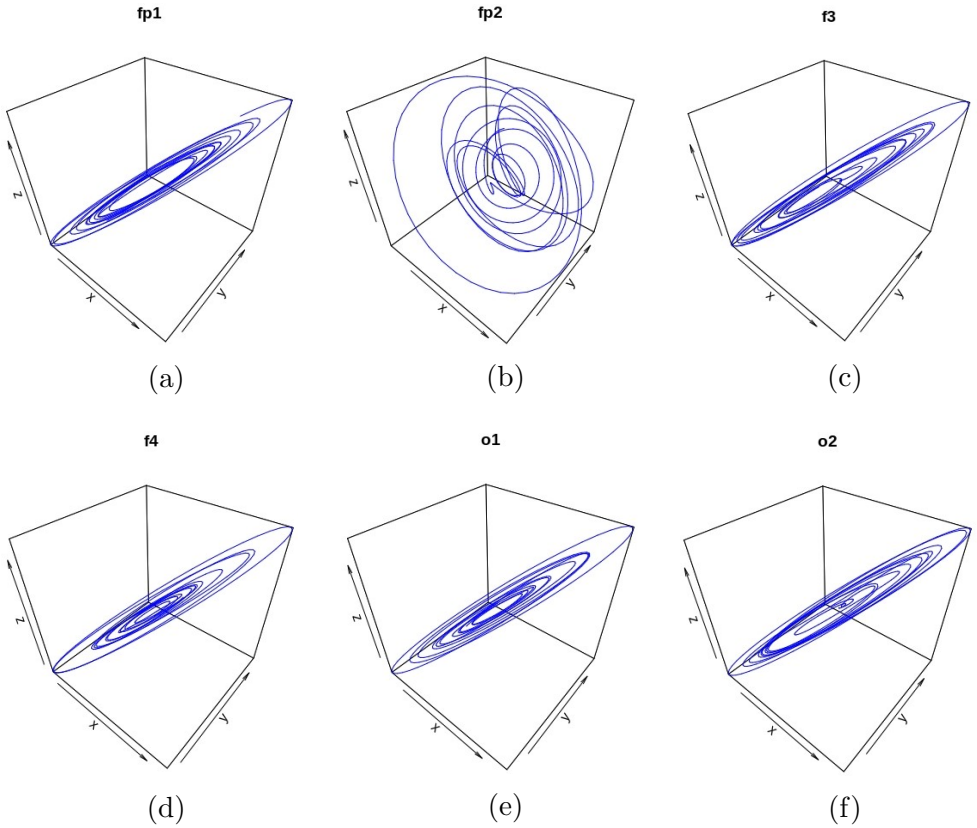

(a) (b) (c)

(d) (e) (f)

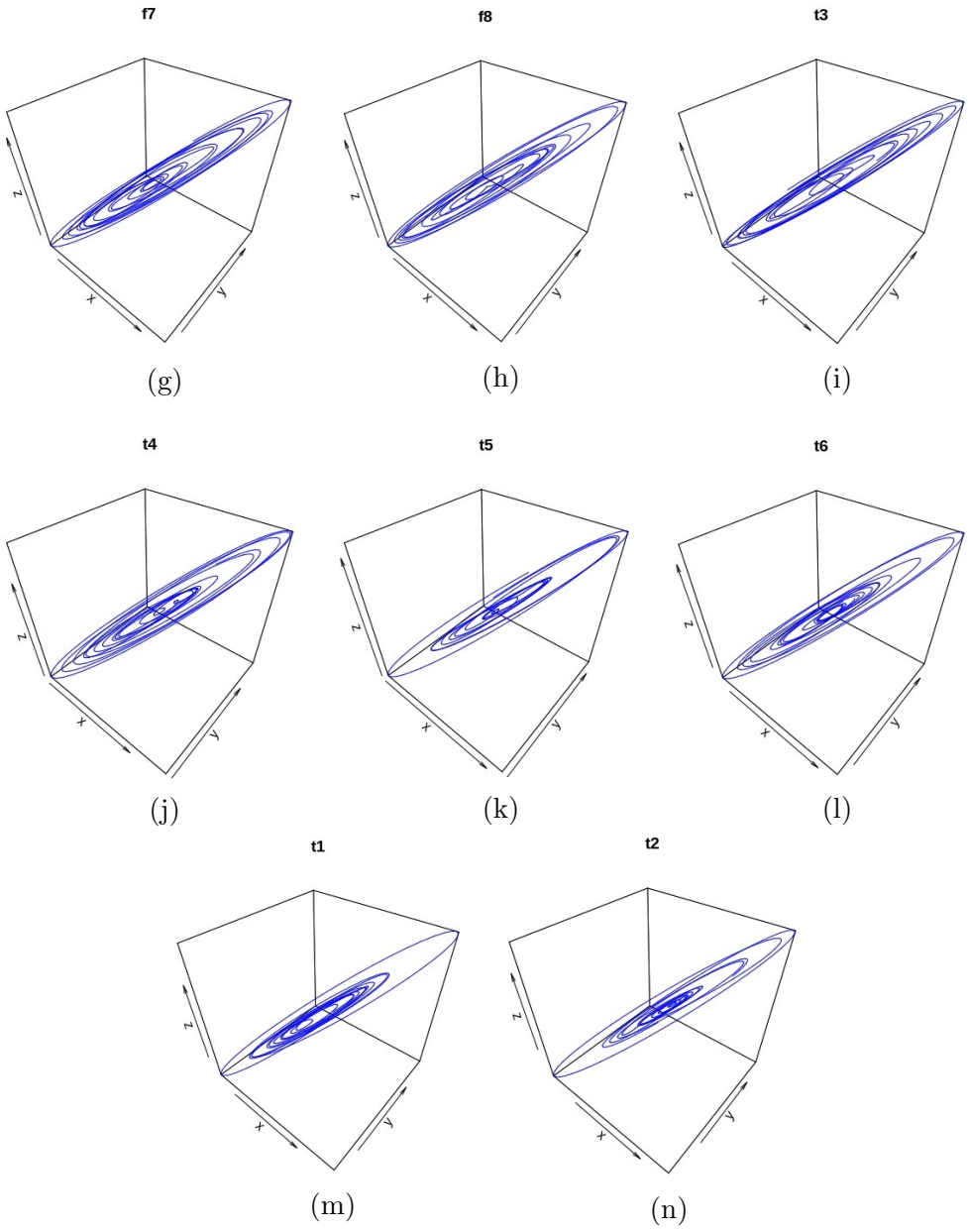

Figure 3.8: Reconstructed Shadow manifold for each Electrode

For each color stimulus, we construct a weighted matrix W_{CCM} with elements w_{ij} as the cross-mapped index from node (electrode) i to j. The obtained connectivity network is directed since W_{CCM} is not symmetric in general. After considering an appropriate threshold value (experimentally chosen as 0.5) for the edge weights, we find the minimum spanning arborescence using **Chu-Liu/ Edmonds' algorithm**[18], which is the directed analogue of minimum spanning tree. Prior to applying the algorithm on the thresholded connectivity network, we subtract 1 from all the non-zero edge weights. The reason for doing so is that by applying Edmonds' algorithm we get a minimum spanning arborescence. However, by subtracting 1 from all the non-zero edge weights, we are essentially converting the relevant maximum weights into minimum weights so that it appears in the minimum spanning arborescence. The weights are then reversed after obtaining the minimum spanning arborescence. The directed graph thus obtained gives information about the direction of maximum information flow. The source of the signals is considered to originate at the occipital lobe, since the stimulus in our experiment is visual. In this experiment, O_2 is chosen as the root for this algorithm. Lastly, from the obtained spanning tree we obtain the probable signal transduction pathways which occur during the presentation of a colored stimulus. Figure 3.9 shows the graph to determine the optimal E and τ for maximum forecasting skill(ρ) of electrode O_1. Reconstructed shadow manifold of each electrode are shown in figure 3.8. From Fig.3.11(a), (b), and (c), we can observe the directed weighted matrices for red, blue and green stimuli respectively, and figure (d) illustrate the spanning arboresence of maximum weight obtained for red stimuli.

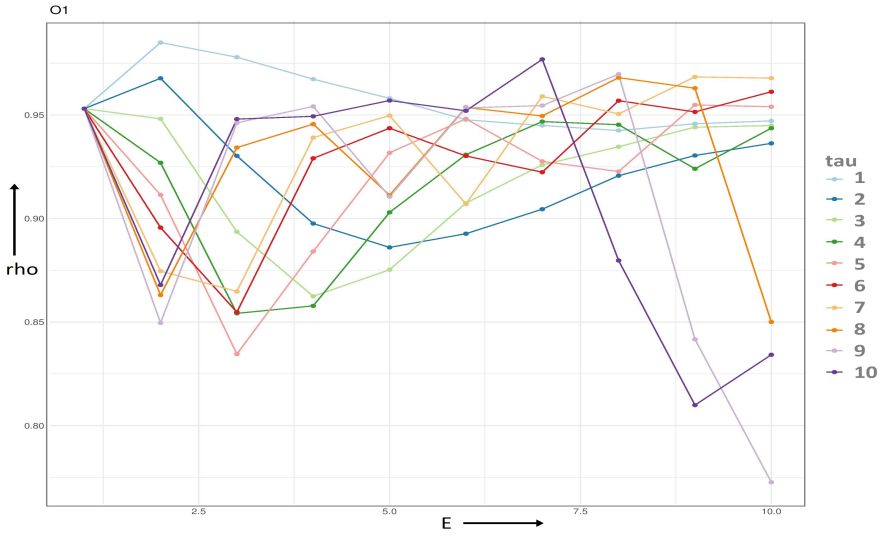

Figure 3.9: Estimation of optimal values of E and τ(tau) for O_1

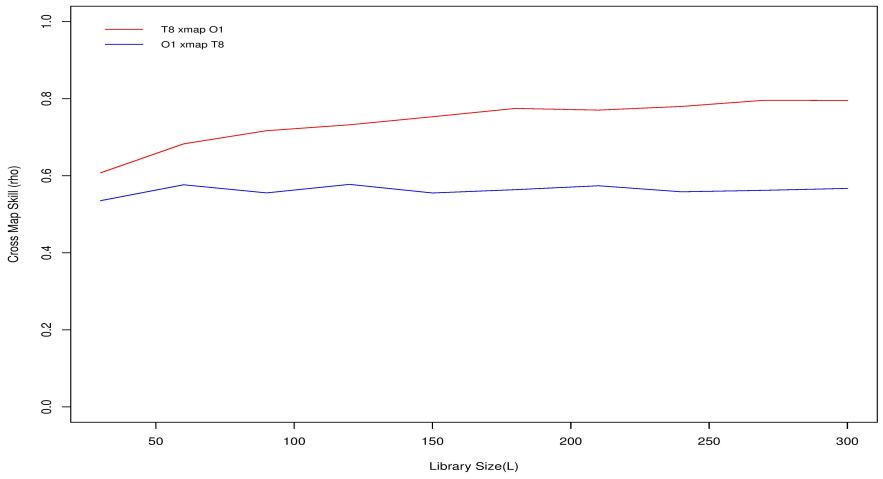

Figure 3.10: Cross mapping skill between T_8 and O_1 over increasing library size (library lengths)

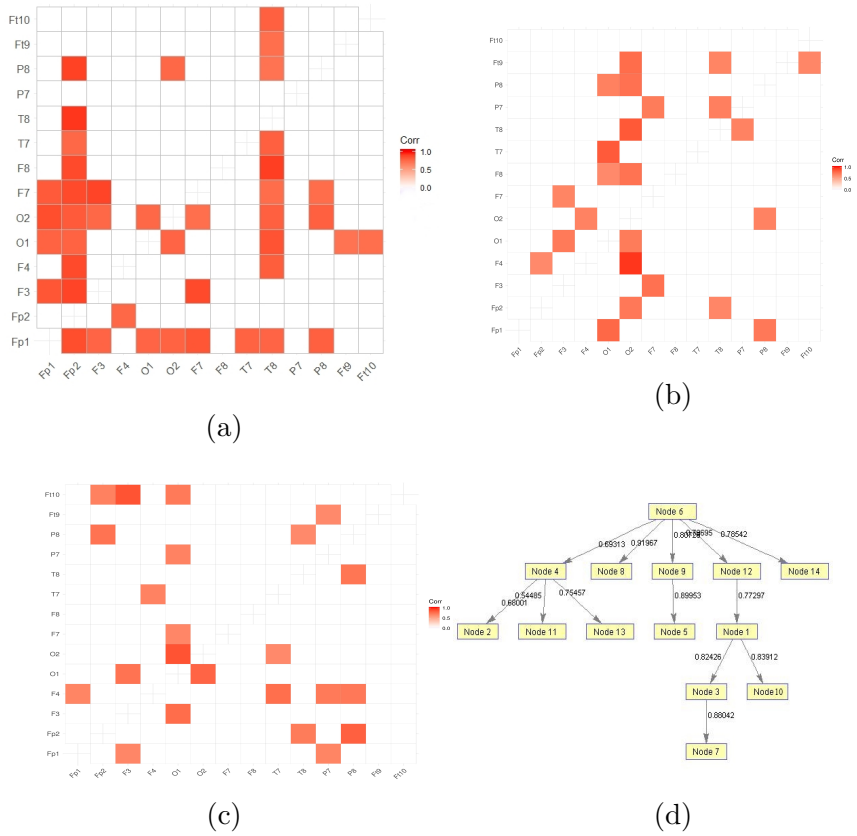

Figure 3.11: (a) Directed weighted matrix W_{CCM} for red stimulus obtained by CCM calculations, (b) Directed weighted matrix W_{CCM} for blue stimulus obtained by CCM calculations, (c) Directed weighted matrix W_{CCM} for green stimulus obtained by CCM calculations, (d) Spanning arborescence of maximum weight obtained for red stimulus by Edmonds' algorithm

3.4 Conclusion

The section examines the scope of CCM in the context of brain connectivity analysis of the well-known color-perception problem. Existing techniques on brain-connectivity analysis highly rely on variants of Granger causality. Unfortunately, Granger causality being a model-dependent technique, as it assumes a linear vector-autoregressive model, is not suitable for brain mapping because of the non-linearity of the EEG signals. CCM, however, is a good choice for non-linear dynamics and thus is an unique technique for the present application. Extensive experiments have been conducted to test the performance of the proposed CCM based brain mapping. Experimental results indicate that the CCM based prediction contains more precise connectivity information, which could not be traced by its competitors.

References

[1] C. W. Granger, "Investigating causal relations by econometric models and cross-spectral methods," *Econometrica: Journal of the Econometric Society*, pp. 424–438, 1969. 46

[2] D. Rathee, H. Cecotti, and G. Prasad, "Estimation of effective fronto-parietal connectivity during motor imagery using partial granger causality analysis," in *2016 International Joint Conference on Neural Networks (IJCNN)*, pp. 2055–2062, IEEE, 2016. 46, 47

[3] R. Kar, A. Konar, A. Chakraborty, and A. K. Nagar, "Detection of signaling pathways in human brain during arousal of specific emotion," in *2014 International Joint Conference on Neural Networks (IJCNN)*, pp. 3950–3957, IEEE, 2014. 46

[4] R. Vicente, M. Wibral, M. Lindner, and G. Pipa, "Transfer entropy—a model-free measure of effective connectivity for the neurosciences," *Journal of computational neuroscience*, vol. 30, no. 1, pp. 45–67, 2011. 46

[5] G. Sugihara, R. May, H. Ye, C.-h. Hsieh, E. Deyle, M. Fogarty, and S. Munch, "Detecting causality in complex ecosystems," *science*, vol. 338, no. 6106, pp. 496–500, 2012. 47, 48, 49, 51, 55

[6] G. Nolte, O. Bai, L. Wheaton, Z. Mari, S. Vorbach, and M. Hallett, "Identifying true brain interaction from eeg data using the imaginary part of coherency," *Clinical neurophysiology*, vol. 115, no. 10, pp. 2292–2307, 2004. 47

[7] J. M. McCracken and R. S. Weigel, "Convergent cross-mapping and pairwise asymmetric inference," *Physical Review E*, vol. 90, no. 6, p. 062903, 2014. 47

[8] C. Luo, X. Zheng, and D. Zeng, "Causal inference in social media using convergent cross mapping," in *2014 IEEE Joint Intelligence and Security Informatics Conference*, pp. 260–263, IEEE, 2014. 47

[9] A. T. Clark, H. Ye, F. Isbell, E. R. Deyle, J. Cowles, G. D. Tilman, and G. Sugihara, "Spatial convergent cross mapping to detect causal relationships from short time series," *Ecology*, vol. 96, no. 5, pp. 1174–1181, 2015. 47

[10] K. Schiecke, B. Pester, D. Piper, F. Benninger, M. Feucht, L. Leistritz, and H. Witte, "Nonlinear directed interactions between hrv and eeg activity in children with tle," *IEEE Transactions on Biomedical Engineering*, vol. 63, no. 12, pp. 2497–2504, 2016. 47

[11] R. D. Pascual-Marqui, C. M. Michel, and D. Lehmann, "Low resolution electromagnetic tomography: a new method for localizing electrical activity in the brain," *International Journal of psychophysiology*, vol. 18, no. 1, pp. 49–65, 1994. 58

[12] R. D. Pascual-Marqui, M. Esslen, K. Kochi, D. Lehmann, *et al.*, "Functional imaging with low-resolution brain electromagnetic tomography (loreta): a review," *Methods and findings in experimental and clinical pharmacology*, vol. 24, no. Suppl C, pp. 91–95, 2002. 58

[13] R. D. Pascual-Marqui, "Discrete, 3d distributed, linear imaging methods of electric neuronal activity. part 1: exact, zero error localization," *arXiv preprint arXiv:0710.3341*, 2007. 58

[14] A. Delorme and S. Makeig, "Eeglab: an open source toolbox for analysis of single-trial eeg dynamics including independent component analysis," *Journal of neuroscience methods*, vol. 134, no. 1, pp. 9–21, 2004. 59

[15] F. Takens, "Detecting strange attractors in turbulence," in *Dynamical systems and turbulence, Warwick 1980*, pp. 366–381, Springer, 1981. 49

[16] K. Pearson, "Vii. note on regression and inheritance in the case of two parents," *proceedings of the royal society of London*, vol. 58, no. 347-352, pp. 240–242, 1895. 54

[17] G. Sugihara and R. M. May, "Nonlinear forecasting as a way of distinguishing chaos from measurement error in time series," *Nature*, vol. 344, no. 6268, p. 734, 1990. 56

[18] J. Edmonds, "Optimum branchings," *Journal of Research of the national Bureau of Standards B*, vol. 71, no. 4, pp. 233–240, 1967. 62

Chapter 4

Decoding Human Decision Making System Using Convolutional Neural Network

Abstract

Human behavior is a complex action which has provoked the thoughts of many people for a long time. However, little is currently known about the origin of cognition and the what defines a person's personality from another. In order to extract the features of a person's personality, we must at first be able to classify them based on their thought processes. In classical ethics, the people can be broadly classified into two main categories, namely, categorical and consequentialist. In this paper, we conduct several experiments where the users are faced with ethical dilemmas and the obtained brain EEG signals are used to classify them in the two categories using a novel modified Covolutional Neural Network. The results show that it is possible to indeed classify the people with extremely high accuracy with only their EEG signals. This provides scope for a new direction of

research which can be explored.

4.1 Introduction

Human behavior has been an intriguing aspect of human cognition and much has gone into the research of finding out why people behave in a particular manner. Though, some great strides have been made in the field, however, it is still unknown to mankind the reason for a particular behavior of man. Many of the decisions happening daily in our culture fall within the category of consequentialist ethics. Consequentialism is an ethical theory that judges whether or not something is right by what its consequences are. For instance, most people would agree that lying is wrong. But if telling a lie would help save a person's life, consequentialism says it's the right thing to do. Consequentialism focuses decision making upon the potential outcomes of an action; the outcome, coupled to some extent with intent, becomes the standard for morality. Consequentialism focuses decision making upon the potential outcomes of an action; the outcome, coupled to some extent with intent, becomes the standard for morality.

In this chapter, we approach a technique to classify the human behavior nature into two class according to their ethical decision making. By consequentialism theory, human behavior can be broadly classified into 2 type; consequential and catagorical. There are several methods exist to classify the EEG signals[1][2][3]. Here we propose a Deep neural[4] network based Convolutional Neural Network(CNN) architecture to complete the task. CNN is basically deals with image data, and used in almost every type of image dataset classification task and different research paper. Recent researches shows that CNN can also be used to classify time series data. Several research paper has been published recently on this topic[5]. So, here we are using CNN as a EEG data classifier

for this experiment. The main idea of this work has been inheritated from[6] [7]. Our experiment shows that CNN gives more accuracy in classification result than the conventional method i.e., KNN,SVM,MLP.

4.2 Methods

Convolutional Neural Network(CNN)[8] is a powerful tool for image data classification. Many image datasets (MNIST,Imagenet, CIFAR10, CIFAR100) classification result shown that CNN outperformed the other classification model by a significant margin. Though CNN is mainly a image based classification model, recently researcher are using CNN for time series classification also. Here in this chapter, we are going to explain the methodology of applying CNN to classify the proposed task.

4.2.1 Our approach

In this section Method for classification the EEG data is discussed briefly. The proposed model is shown in the Figure 3.1

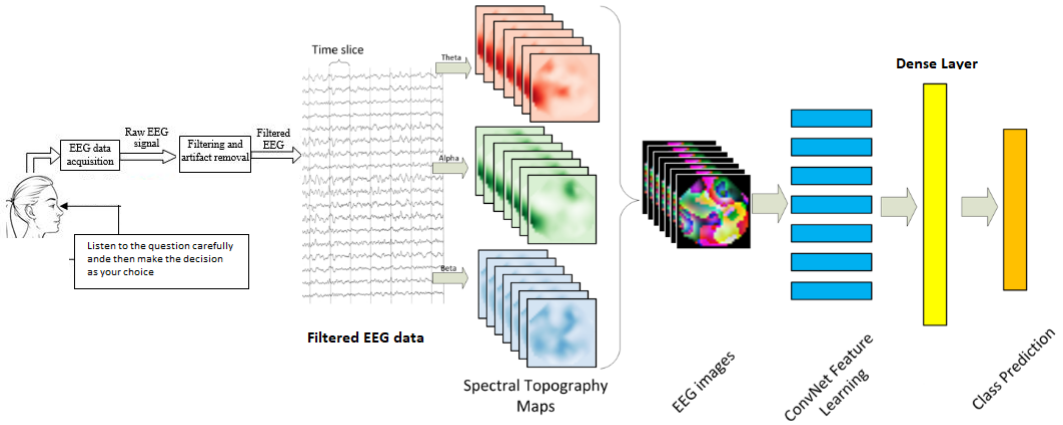

Figure 4.1: Model Architecture

4.2.1.1 Generating image from EEG data

Electroencephalogram(EEG), measures the signals generated from the different brain regions, with the help of several electrodes placed around the cortex. Although, EEG signals have spatial dimension, but most of the significant features are extracted from the frequency domain. The reason behind this is EEG has very high temporal resolution[9]. For decision making, the frequency bands involved are mainly theta(4-8Hz), alpha(8-14Hz) and beta(14-30Hz)[10].So, we are taking Fast Fourier Transform(FFT) of the EEG signals in three different frequency band ranges for each trial. Now we assign the value of each electrode with the mean of the squared absolute value of three different frequency bands. These values can be plotted within a 2D topographical map to form an image[7]. With consecutive time windows, we can create temporal evolution of the EEG signal in a form of sequential image.

EEG electrodes are placed in a 3D space in human scalp. So to generate a 2D image of the topographical map, we have to be careful about the relative distance between the electrodes when projecting the 3D location in a 2D plane. To do so, Azimuthal Equidistance Projection(AEP)[11] also known as Polar Projection is employed here. The most important property of AEP is that it preserves the distance and direction intact from the center as it was in the 3D surface. Figure 1 shows the electrode location in 3D space and its 2D projection.

Akima interpolation[12] method is applied here to estimate the value in between the two electrode to get a smooth image of topographical map. Repeating this procedure for three different frequency bands we are working with, we get three different topographical images(3 channels) for a single trial. These three images can be interpreted as the three channels(RGB) for color images and given as input of a CNN. CNN is explained in the following section.

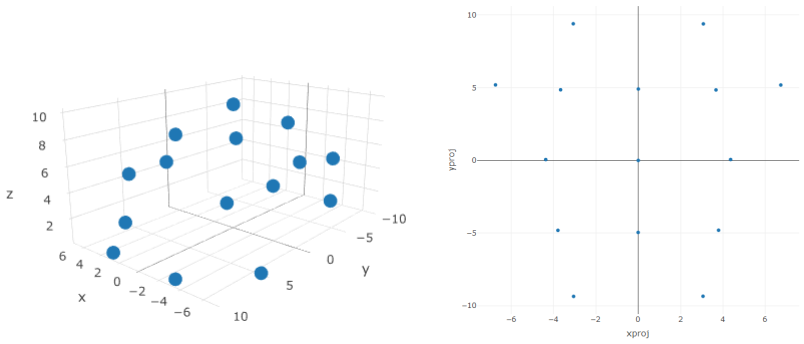

(a) 3D plot of electrode locations

(b) 2D projection of the electrode locations

4.2.1.2 Convolutional Neural Network

Here CNN is employed as a classifier to classify the images generated from the EEG signals. These images are generated by processing the 15 channel EEG data into a frame of one second window and then a 2D projection of scalp is made from this frame. In a CNN, convolution, pooling, dropout, fully connected layers exist. The model here in this experiment is implemented using tensorflow and Keras[13] library in Python. In our model we use 4 convolution layers, 3 pooling layers and 2 dense layers. Rectifier linear unit(ReLU) is used as an activation function in the convolution layer and "softmax" in the output layer. We take all the images generated from the EEG signals as input images. Then first Convolution operation is made by 32 filter with dimentions of 3*3. This filter size is fixed for all the convolution layers in this model with a stride of 1 pixel. We are using zero padding to keep the dimension of the input image intact after the convolution operation. Next we take another Convolution layer followed by a MaxPooling layer. The pooling operation is here MaxPooling of 2*2 window size with a stride of 1 pixel. Next, we take 2 more convolution layers followed by a maxpooling layer after each convolution layer before adding a fully connected dense layer. The length of convolution filter is increased every time it

goes into deeper layer. The more we go deep into the network, image resolution becomes smaller and better features are extracted. Finally, we create a dense layer of output dimension. In this layer, we use "softmax" as the activation layer. Softmax layer give the predicted class for a given input by checking the maximum probability distribution from the output layer. We use categorical cross-entropy as a loss function and adam optimizer[14] with learning rate 0.0001 to train the model.

To understand the operation of the layers better, a illustrated example is summarized here. We are taking 3 channel RGB color image in this example. Let, the dimensions of the image be (W_1*H_1*D_1), where W_1, H_1 and D_1 are the width, height, and channel of the input image respectively. Now, the parameter required to perform the operations are:

1. Number of filters K,
2. Filter size F,
3. The stride S,
4. The amount of zero padding P.

After convolution operation, it produces a volume of size (W_2xH_2xD_2), where, $W_2 = (W_1 - F + 2P)/S + 1$, $H_2 = (H_1 - F + 2P)/S + 1$ and $D_2 = K$.

Figure 4.3 shows the complete operation of the convolution layer in details. It shows that the input image is convolved with the filter size of 3*3 with a stride of 2, for the entire input image. Each element of the highlighted area of input image(blue) is multiplied with the filter element(red) and then summed up along with the bias to produce the output value of the highlighted element(green).

Next pooling layer is taking the output of the convolution layer as an input and extracting the best feature by reducing the output image dimension. We are

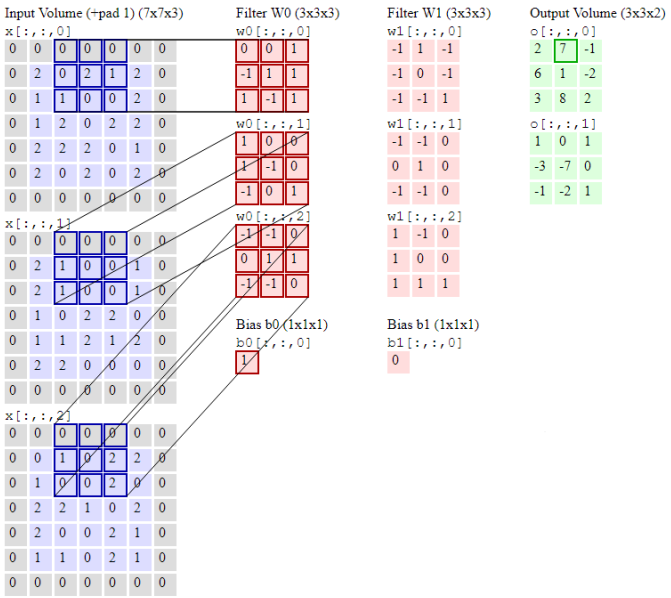

(a)

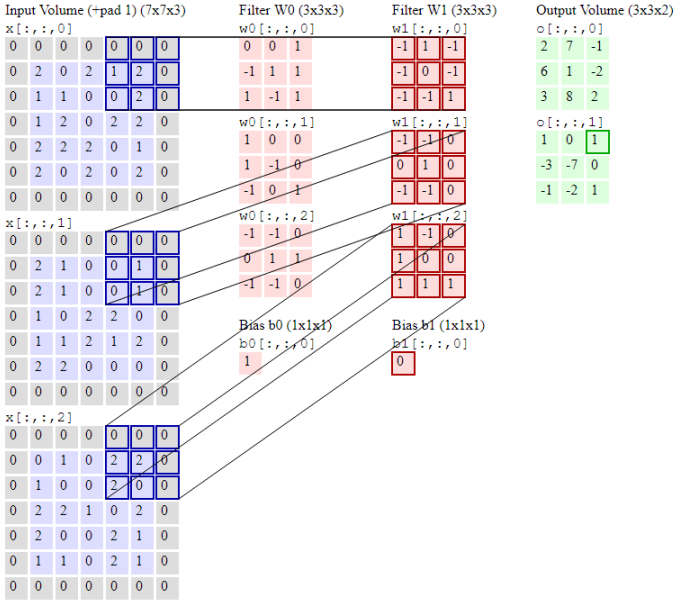

(b)

Figure 4.3: Convolution layer operation

using maxpool as the pooling layer operation. Figure 4.4 shows the pooling layer operation briefly

4.2.2 Classification of Persons based on Decisions

According to the types of moral decision a person makes, he can be broadly classified into two broad categories viz., Categorical and Consequential. While on one hand, categorical decision making locates morality in certain duties and rights, according to the consequentialist theory, people who fall in that category locates morality in the consequences of the act.

4.3 Experiment

4.3.1 Participants

Eighteen healthy participants (8 female), aged 23.22±2.98 years and all attending college or graduated. The subjects had no diagnosis of neurological (ICD-10: G00-G99), psychiatric (ICD-10: F00-F99), and/or motor diseases (ICD-10: M00-M99) and had normal or corrected-to-normal vision. Ethical approval was obtained from the local Ethics Committee and participants provided written con-

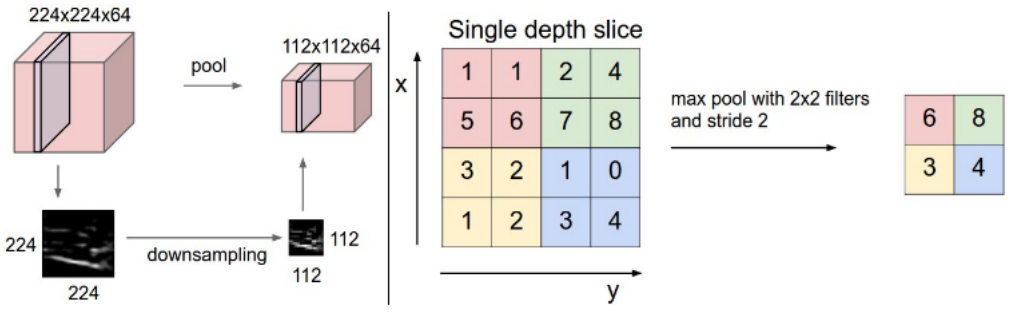

Figure 4.4: MaxPool operation to downsample the image

sent prior to participation and the experiments were conducted according to the Helsinki protocol[].

4.3.2 Data Acquisition

The recording was performed using a 72-channel Nihon Kohden system, with a sampling frequency of 500 Hz, Germany) with 32 positioned electrodes according to the 10- 20 system arranged in Fp1, Fp2, F7, F3, Fz, F4, F6, FC5, FC3, FC1, FC2, FC4, FC6, T7, C3, Cz, C4, T8, CP5, CP3, CP1, CP2, CP4, CP6, P7, P3, Pz, P4, P8, O1, Oz, O2. The reference was FCz, and the ground was AFz.

4.3.3 Ethical Decision Task

The ethical questions were inspired from the first lecture of the Harvard course on Justice by Prof Michael Sandel titled "THE MORAL SIDE OF MURDER".

4.3.3.1 Scenario 1

In the first scenario, we gave the subjects the classic runaway railroad problem. In the scenario, there is a railway engine whose control is lost and is heading towards a junction. The subject is put into a hypothetical situation where he is an observer and has a lever in front of him which can change the course of the runaway railway engine. Moreover, the situation also entails that if the user does not switch the handle and the engine is let to run its free course, it will kill 5 people who are there on the tracks. On the other hand, if the lever is pulled, the tracks will change and as a result only 1 person will die. The subject was then asked the first ethical question whether he would like to pull the lever or let it be if such a situation ever arose.

4.3.3.2 Scenario 2

In the next scenario, the point of view of the subject is changed. In this case, there is no lever which the subject has to pull and instead, he is watching the runaway train from a bridge overhead and is accompanied by a huge man. The situation is such that the subject knows that if he pushes that big man to fall on the tracks, he would die but stop the train and save the lives of the 5 people working on the tracks. The subject is then asked the question whether he or she would be likely to push the man. This, though logically has the same logic of killing one person to save five, has different results as the person is the directly involved in killing somebody. After this, question, the subject was farther asked what he would do if instead of pushing, he indeed had a lever which he could pull to kill the person like the former case.

4.4 Data preprocessing

Performance measure: The performance of each participant was calculated after ocular correction and removal of trials with overt muscle movements.

4.4.0.1 Ocular correction

To eliminate interference from eye movement and blinks, we applied Independent Component Analysis (ICA), using Brain Vision Analyzer 2.0 (Brain Products GMDH, Germany). First the sampling rate was changed to 250 Hz, and then the data were bandpass filtered between 1 and 50 Hz. The signal was then segmented into 9.0s epochs (Figures 1B and C) representing blocks of classifier training and those of the main task. Although only the trials of the main task were used in further analysis, all blocks were segmented for increasing the number of samples used in the ICA correlation. ICA analysis then decomposes the data into 32

components which are visually analyzed for those that resemble eye artefacts.

4.4.0.2 Removal of trials with muscle movement

To eliminate those trials where the participants moved, the signal of EEG electrodes were segmented into periods of baseline and those of motor imagery. These segments were then filtered with a high pass 7th order Butterworth filter at 10 Hz and subsequently rectified (extraction module). The baseline epochs were then examined using windows of 0.3 s, moving along the data with steps of 0.15 s. From these windows a root mean square (RMS) baseline EEG was calculated. Each trial was examined in the same way, and a mean and standard deviation of baseline EEG RMS was calculated for each participant. The motor imagery periods were pre-processed in the same way as the baseline to create RMS values. Trials where the RMS exceeded the baseline mean + 1.96 of the standard deviation were excluded as having muscle movement. The average number of rejections 24.56±31.26 of 160 trials.

4.5 Results

In this section, we compare the result we achieve with the existing other popular classification models like, KNN, SVM, MPL. Then we also compare the result of our model with tuning the hyperparameter. The classification accuracy of different model are illustrated in the table 4.1.

From Table 4.1 we can see that CNN classifier model gives the best accuracy among all the classifiers being tested. So we choose CNN as our primary classifier model here. Now we can boost the performance of our model by tuning the parameter of the model architecture. Comparison between these modified CNN are given in the table 4.2.

Table 4.1: Comparison of different classifier model

Classifier	Training Accuracy	Validation accuracy
KNN	58.6	52.34
SVM	72.91	68.8
MLP	76.47	70.26
CNN	82.45	78.39

Table 4.2: Comparison of tuned parameter model of CNN

Number of filter	**Filter size**	**Pooling size**	**Optimize**	**Epoch**	**Accuracy**
32,80,200	3*3,3*3,3*3	None,2*2,2*2	SGD	300	78.9
32,80,200	3*3,3*3,3*3	None,2*2,2*2	Adam	300	84.56
32,80,200	3*3,3*3,3*3	None,2*2,2*2	SGD	400	87.88
32,80,200	3*3,3*3,3*3	None,2*2,2*2	Adam	400	88.54
32,80,200	4*4,4*4,4*4	None	SGD	400	89.34
32,80,200	4*4,4*4,4*4	None	Adam	400	91.67

Table 4.2 shows that the model without any pooling layer gives the best accuracy. The size of the filter in this model is larger than the size where the model is trained with pooling layer. The optimizer choosen here is Adam and this model gives us accuracy of 91.67%.

4.6 Conclusion

The human behavior can be classified into 2 class as discussed earlier in this chapter. So, we make a approach to correctly classify those to type of human mental state. EEG data has been taken during some ethical decision making problem. According to theory of consequentialism, we can classify human behaviour from the answer they have choose. So, we label the answer according to that, and try to put that EEG data into a CNN based classifier. Our method showed a

great result to classify the data we get. Nearly 92% accuracy has been achieved with our CNN based classifier model. Though CNN is mainly an image based classifier, we can also use this model to classify the time series EEG data by creating topographical image of the brain activation of different frequency band. This classifier gives also better result than conventional classifier model.

References

[1] A. Craik, Y. He, and J. L. P. Contreras-Vidal, "Deep learning for electroencephalogram (eeg) classification tasks: A review," *Journal of neural engineering*, 2019. 69

[2] F. Lotte, L. Bougrain, A. Cichocki, M. Clerc, M. Congedo, A. Rakotomamonjy, and F. Yger, "A review of classification algorithms for eeg-based brain–computer interfaces: a 10 year update," *Journal of neural engineering*, vol. 15, no. 3, p. 031005, 2018. 69

[3] F. Lotte, M. Congedo, A. Lécuyer, F. Lamarche, and B. Arnaldi, "A review of classification algorithms for eeg-based brain–computer interfaces," *Journal of neural engineering*, vol. 4, no. 2, p. R1, 2007. 69

[4] D. E. Rumelhart, G. E. Hinton, and R. J. Williams, "Learning internal representations by error propagation," tech. rep., California Univ San Diego La Jolla Inst for Cognitive Science, 1985. 69

[5] "A deep learning method for classification of eeg data based on motor imagery," *Intelligent Computing in Bioinformatics*, p. 203, 2014. 69

[6] J. Y.-H. Ng, M. Hausknecht, S. Vijayanarasimhan, O. Vinyals, R. Monga, and G. Toderici, "Beyond short snippets: Deep networks for video classifica-

tion," *2015 IEEE Conference on Computer Vision and Pattern Recognition (CVPR)*, Jun 2015. 70

[7] P. Bashivan, I. Rish, M. Yeasin, and N. Codella, "Learning representations from eeg with deep recurrent-convolutional neural networks," 2015. 70, 71

[8] Y. LeCun, Y. Bengio, *et al.*, "Convolutional networks for images, speech, and time series," *The handbook of brain theory and neural networks*, vol. 3361, no. 10, p. 1995, 1995. 70

[9] A. Gevins, H. Leong, M. E. Smith, J. Le, and R. Du, "Mapping cognitive brain function with modern high-resolution electroencephalography," *Trends in neurosciences*, vol. 18, no. 10, pp. 429–436, 1995. 71

[10] G. Deuschl, A. Eisen, *et al.*, "Recommendations for the practice of clinical neurophysiology: guidelines of the international federation of clinical neurophysiology," 1999. 71

[11] P. S. Anderson, "An oblique, poly-cylindrical, orthographic azimuthal equidistant cartographic projection: its purpose, construction and theory," *Cartography*, vol. 8, no. 4, pp. 182–186, 1974. 71

[12] H. Akima, "A new method of interpolation and smooth curve fitting based on local procedures," *Journal of the ACM (JACM)*, vol. 17, no. 4, pp. 589–602, 1970. 71

[13] F. Chollet *et al.*, "Keras," 2015. 72

[14] D. P. Kingma and J. Ba, "Adam: A method for stochastic optimization," *arXiv preprint arXiv:1412.6980*, 2014. 73

Chapter 5

Conclusions

5.1 Self Review

The Thesis attempts to offer an interesting and useful solution to the well-known problem of determining signal transduction pathways among the brain lobes during a cognitive task and classification of the pattern activation of EEG signals. A Granger causality based analysis is undertaken to determine the directed pathways in the graphs obtained by phase-synchrony analysis. Experiments undertaken confirm that for 3 basic colors, the signal transduction pathways are different. Though Granger causality test is only applicable for stationary time series data, we perform this test here by taking the first difference of the EEG data, as we know EEG data is non-stationary and dynamic in nature. So, sometimes this test gives false positive results. To overcome this problem we use a relatively new method called Convergent Cross Mapping(CCM). This technique is full functional for non-stationary and dynamical system data. If a two time series data are from a same dynamical system then their individual reconstructed shadow manifold have a one to one mapping with the original dynamical system manifold. The signaling pathway is determined by checking the causality between different brain lobes. So, we check the causality of the electrodes with the help of cross map skill by simplex projection. After checking the result we can see that more

precise pathway can be derived from the CCM method.

On the other hand, a classification task is performed to determine the human behavior on the basis of their thought process and decision making. We use a Deep Convolutional Neural Network as our classifier model. Human behavior can be classified broadly into two category, Categorical and Consequentialist. Comparing with other conventional EEG signal classifier we can observe that our CCN based model gives significantly higher classification accuracy.

5.2 Future Work

From the chapter 4, the data taken from the EEG signals to perform the task is free from any emotional attachment. We take the data of the different scenario with general decision making process, which make the task easier when comparing with a situation where emotional involvment is there. Our future work will be progress into that way where various external factor will be added when making a ethical decision.

Recently researcher create BrainNet, which is the first multi-human non-invasive direct brain-to-brain interface for collaborative problem solving. The interface combines electroencephalography (EEG) to record brain signals and transcranial magnetic stimulation (TMS) to deliver information non-invasively to the brain. The interface allows three human subjects to collaborate and solve a task using direct brain-to-brain communication. Two of the three subjects are designated as "Senders" whose brain signals are decoded using real-time EEG data analysis. The decoding process extracts each Sender's decision about whether to rotate a block in a Tetris-like game before it is dropped to fill a line. The Senders' decisions are transmitted via the Internet to the brain of a third subject, the "Receiver," who cannot see the game screen. The Senders' decisions are delivered to the Receiver's brain via magnetic stimulation of the occipital cortex.

The Receiver integrates the information received from the two Senders and uses an EEG interface to make a decision about either turning the block or keeping it in the same orientation. A second round of the game provides an additional chance for the Senders to evaluate the Receiver's decision and send feedback to the Receiver's brain, and for the Receiver to rectify a possible incorrect decision made in the first round. We are aiming to figure out a connectivity mapping of EEG signals during decision making process, so that this type of technology can get more precise when in operation.